CHEMICAL ABUNDANCES OF THREE METAL-POOR GLOBULAR CLUSTERS (NGC 6287, NGC 6293, AND NGC 6541) IN THE INNER HALO

Jae-Woo Lee 1,2,3,4 and Bruce W. Carney 1,4

ABSTRACT

We present a chemical abundance study of three inner old halo clusters NGC 6287, NGC 6293, and NGC 6541, finding [Fe/H] = -2.01 ± 0.05 , -1.99 ± 0.02 , and -1.76 ± 0.02 (internal), respectively, and our metallicity measurements are in good agreement with previous estimates. We also present the radial velocity measurements of the clusters. Our radial velocity measurements for NGC 6293 and NGC 6541 are in good agreement with previous measurements, however, our radial velocity measurement for NGC 6287 is almost 80 km s⁻¹ larger than the previous measurement.

The mean α -element abundances of our program clusters are in good agreement with other globular clusters, confirming previous results. However, the individual α -elements appear to follow different trends. The silicon abundances of the inner halo clusters appear to be enhanced and the titanium abundances appear to be depleted compared to the intermediate halo clusters. Our results also appear to oppose to those of metal-rich bulge giants studied by McWilliam and Rich, who found that bulge giants are titanium enhanced and silicon deficient. In particular, [Si/Ti] ratios appear to be related to Galactocentric distances, in the sense that [Si/Ti] ratios decrease with Galactocentric distance. We propose that

¹Department of Physics & Astronomy, University of North Carolina, Chapel Hill, NC 27599-3255; jae-woo@astro.unc.edu; bruce@physics.unc.edu

²Center for Space Astrophysics, Yonsei University, Shinchon-dong 134, Seoul 120-749, Korea

 $^{^3\}mathrm{PMA}$ Division, California Institute of Technology, Mail Stop 405-47, Pasadena, CA 91125, USA; jaewoo@srl.caltech.edu

⁴Visiting Astronomer, Cerro Tololo Inter-American Observatory, National Optical Astronomy Observatories, which are operated by the Association of Universities for Research in Astronomy, Inc., under contract with the National Science Foundation.

contributions from different masses of the SNe II progenitors that enriched protoglobular cluster clouds' elemental abundances and the different initial physical environments surrounding the proto-globular clusters clouds are responsible for this gradient in [Si/Ti] ratios versus Galactocentric distances of the "old halo" globular clusters. On the other hand, our program clusters' enhanced s-process elemental abundances suggest that the formation timescale of our program clusters might be as short as a few times 10^8 yr after the star formation is initiated in the Galaxy's central regions, if the s-process site is intermediate mass AGB stars.

Subject headings: Galaxy: halo — globular clusters: individual (NGC 6287, NGC 6293, NGC 6541) — stars: abundances

1. INTRODUCTION

Detailed elemental abundance studies of globular clusters may provide strong constraints on the Galaxy formation picture. For example, a metallicity gradient would imply that the Galaxy formed via a slow dissipational process. A constant and enhanced $[\alpha/\text{Fe}]$ versus [Fe/H] relation may indicate that the globular clusters must have formed simultaneously within a couple of gigayears (Wyse & Gilmore 1988; Wheeler et al. 1989; Carney 1996), so that their proto-globular cluster clouds (PGCCs) were not contaminated by SNe Ia products. The abundance ratio of r-process elements to s-process elements, such as [Ba/Eu] and [La/Eu], as a function of metallicity in globular cluster systems, may also suggest how rapidly they were polluted by the low- or intermediate-mass stars before they formed.

In spite of the importance of the chemical abundance studies, few high resolution spectroscopic studies of the globular clusters near the Galactic center have been performed due to the observational limitations set by large interstellar reddening. Geisler (1988) studied NGC 6541 employing the Washington photometric system and obtained $[Fe/H] = -0.99 \pm 0.20$. The high metallicity for NGC 6541 led Geisler (1988) to claim that NGC 6541 is the one of the examples of the second parameter problem since it has a BHB morphology for its metallicity. Rutledge et al. (1997a) studied NGC 6541 using the Ca II triplet with low resolution spectra and obtained $[Fe/H] = -1.79 \pm 0.02$ on the Zinn & West (1984) metallicity scale. In this case, a second parameter is unnecessary to explain the HB morphology of NGC 6541. Kennedy, Bates, & Kemp (1998) employed high resolution spectroscopy for several stars in NGC 6541, but their study focused on the interstellar medium towards NGC 6541 using spectral regions near Na I D lines.

In this paper, we explore the detailed elemental abundances for RGB stars in the metalpoor inner halo globular clusters NGC 6287 ($R_{GC} = 1.6 \text{ kpc}$), NGC 6293 ($R_{GC} = 1.4 \text{ kpc}$), and NGC 6541 ($R_{GC} = 2.2 \text{ kpc}$) using high resolution spectra. Lee et al. (2001) and Lee, Carney, & Heasley (2002, in preparation) employed HST NIC3 and PC2 photometry of these clusters to show that they essentially have the same age as the one of the oldest globular clusters in our Galaxy, M92. A comparative elemental abundance study between these three clusters and the intermediate halo clusters (or the metal-poor halo stars) will provide clues of the early chemical enrichment history of the inner part of our Galaxy.

2. OBSERVATIONS AND DATA REDUCTION

We selected our program RGB stars from Stetson & West (1994), Janes & Heasley (1991), and Alcaino (1979) for NGC 6287, NGC 6293, and NGC 6541, respectively. We obtained high S/N (\geq 95) echelle spectra using the CTIO 4-meter telescope and its Cassegrain echelle spectrograph. The Tek 2048 × 2048 CCD, 31.6 lines/mm echelle grating, long red camera, and G181 cross-disperser were employed for our observations. The slit width was 150 μ m, or about 1.0 arcsec, that projected to 2.0 pixels and which yielded an effective resolving power R=28,000. Each spectrum had complete spectral coverage from 5500 to 7850 Å for the 1998 run and 5700 to 8000 Å for the 1999 run. All program star observations were accompanied by flat lamp, Th-Ar lamp, and bias frames. We also obtained spectra of rapidly rotating early type stars in order to remove telluric absorption features. During the 1998 run, the seeing conditions were extremely poor, no better than 2-2.5 arcsec for 5 nights. The seeing conditions were slightly better, with the mean of 1.5 arcsec, during the 1999 run. The basic photometric data for the program RGB stars and the journal of observations are given in Table 1.

The raw data frames were trimmed, bias-corrected, and flat-fielded using the IRAF⁵ ARED and CCDRED packages. The scattered light was also subtracted using the AP-SCATTER task in ECHELLE. The echelle apertures were then extracted to form 1-d spectra, which were continuum-fitted and normalized, and a wavelength solution was applied following the standard IRAF echelle reduction routines. The telluric line removal was performed by dividing a program star spectrum by that of rapidly rotating early type stars.

Equivalent widths were measured mainly by the direct integration of each line profile

⁵IRAF (Image Reduction and Analysis Facility) is distributed by the National Optical Astronomy Observatory, which is operated by the Association of Universities for Research in Astronomy, Inc., under contract with the National Science Foundation.

using the SPLOT task in IRAF ECHELLE package. The equivalent widths for our program stars are listed in Table 2.

3. ANALYSIS

In our elemental abundance analysis, we use the usual spectroscopic notations that $[A/B] \equiv \log(N_A/N_B)_{star} - \log(N_A/N_B)_{\odot}$, and that $\log n(A) \equiv \log(N_A/N_H) + 12.00$ for each element. For the absolute solar iron abundance, we adopt $\log n(\text{Fe}) = 7.52$ following the discussion by Sneden et al. (1991).

3.1. Line Selection and Oscillator Strengths

For our line selection, laboratory oscillator strengths were adopted whenever possible, with supplemental solar oscillator strength values. In addition to oscillator strengths, taking into account the damping broadening due to the van der Waals force, we adopted the Unsöld approximation with no enhancement. We list the source of oscillator strengths in Table 3.

The abundance analysis mainly depends on the reliability of the oscillator strength values for the Fe I and Fe II lines, since not only the metallicity scale but also the stellar parameters, such as spectroscopic temperature, surface gravity, and microturbulent velocity, will be determined by using these lines. We mainly relied upon the extensive laboratory oscillator strength measurements by the Oxford group (Blackwell et al. 1979; 1982b, 1982c, 1986a). We also used oscillator strength values measured by O'Brian et al. (1991) and the Hannover group (Bard, Kock, & Kock 1991; Bard & Kock 1994). In our iron abundance analysis, we consider the Oxford group's measurements (the absorption method) as primary oscillator strengths and oscillator strength measurements that relied on emission methods (O'Brian et al. 1991; Bard, Kock, & Kock 1991; Bard & Kock 1994) as supplemental. Therefore, the oscillator strengths by O'Brian et al. and the Hannover group were scaled with respect to those by the Oxford group as a function of excitation potential (de Almeida 2000, private communication),

$$\log gf = \log gf(OB) - 0.017,$$

$$\log gf = \log gf(H91) - 0.015 - 0.009\chi,$$

$$\log gf = \log gf(H94) - 0.027 - 0.009\chi,$$
(1)

where the excitation potential χ is given in electron volts. Blackwell, Smith, & Lynas-Gray (1995) also pointed out that there appears to exist a slight gradient in the excitation potential

between oscillator strengths by the Oxford group and those by the Hannover group, with $\log gf(Oxford) = \log gf(Hannover) - 0.021 - 0.006\chi$.

For neutral titanium lines, we relied on the laboratory measurements by the Oxford group (Blackwell et al. 1982a, 1983, 1986b). It should be noted that the original Oxford gf-values have been increased by +0.056 dex following Grevesse, Blackwell, & Petford (1989). They discussed that their original gf-values relied on the inaccurate lifetime measurements and the absolute gf-values should be revised based on the new measurements.

Contrary to other elements possessing HFS components, HFS components should be considered in the barium abundance analysis because Ba II lines are usually very strong even in metal-poor stars and the desaturation effects due to HFS components become evident (see for example, McWilliam 1998). We adopted the Ba II HFS components and oscillator strengths of Sneden et al. (1997). Note that Sneden et al. (1997) did not publish their HFS line list but the electronic version of Ba II HFS components was kindly provided by Chris Sneden and Inese Ivans (2000, private communication).

3.2. Stellar Parameters and Model Atmospheres

Having good stellar parameters, such as the effective temperature and the surface gravity, is very important in any stellar abundance study, since the absolute or the relative elemental abundance scale will depend on the input stellar parameters. For our analysis, we rely on spectroscopic temperatures and photometric surface gravities.

The initial estimates of the temperature of program stars were estimated using BV photometry of our program clusters (Stetson & West 1994, Janes & Heasley 1991, and Alcaino 1979, for NGC 6287, NGC 6293, and NGC 6541, respectively) and the empirical color-temperature relation given by Alonso, Arribas, & Martinez-Roger (1999). Since their relation depends slightly on the metallicity, we adopted [Fe/H] = -2.05, -1.90, and -1.80 for NGC 6287, NGC 6293, and NGC 6541 (Harris 1996). To estimate the dereddened color, we adopt E(B-V) = 0.62, 0.40, and 0.14 for NGC 6287 (Lee et al. 2001), NGC 6293, and NGC 6541 (Lee, Carney, & Heasley 2002, in preparation), respectively (see also Table 4). It should be noted that our E(B-V) values are estimated using HST NIC3 photometry (NGC 6287) and PC2 photometry (NGC 6293 and NGC 6541) are in good agreement with those of Harris (1996) to within 0.02 mag. Our program clusters have large interstellar reddening values because they are located near the Galactic center and they even suffer from

the differential reddening.⁶ Therefore, the uncertainty in the interstellar reddening is the major source of error in our photometric temperature estimation. Generally, an uncertainty of 0.1 mag in E(B-V) results in an uncertainty of $\approx 100-130$ K in photometric effective temperature.

To derive photometric surface gravity in relation to that of Sun, we use $\log g_{\odot} = 4.44$ in cgs units, $M_{bol,\odot} = 4.74$ mag, and $T_{eff,\odot} = 5777$ K for the Sun (Livingston 1999) and we assume the stellar mass $M = 0.8~M_{\odot}$. We use the empirical relation given by Alonso et al. (1999) to estimate the bolometric correction. We adopt $(m-M)_0 = 14.35$, 14.61, and 14.19 mag for NGC 6287 (Lee et al. 2001), NGC 6293, and NGC 6541 (Lee, Carney, & Heasley 2002, in preparation). Our $(m-M)_0$ values are 0.30, 0.11, and 0.05 mag smaller than those of Harris for NGC 6287, NGC 6293, and NGC 6541, respectively. In general, an uncertainty of 0.3 mag in $(m-M)_0$ results in an uncertainty of 0.1 dex in $\log g$, in the sense that a short distance scale results in a high surface gravity.

As an independent test, we compared the spectroscopic temperature and surface gravity of M92 RGB stars by Sneden et al. (1991) to those calculated using the photometric method above. Using M92 RGB stars provides an advantage that the interstellar reddening towards M92 is negligibly small, E(B-V)=0.02. Thus, the uncertainty raised by the interstellar reddening in the photometric temperature and surface gravity estimates will be minimized. Our calculations showed that the photometric and spectroscopic temperature scales are in very good agreement with $\Delta[T_{eff}(\text{spectroscopic}) - T_{eff}(\text{photometric})] = 37 \pm 11$ K. We calculate the photometric surface gravity for $0.80~M_{\odot}$ and $0.85~M_{\odot}$, which are roughly the stellar evolutionary mass for the RGB stars in the oldest metal-poor clusters (Bergbusch & VandenBerg 2001). Both cases are in very good agreement with the surface gravity measurements by Sneden et al. (1991). For our photometric surface gravity estimates, a stellar mass of $0.80~M_{\odot}$ is assumed for each program star.

With initial photometric temperature and surface gravity estimates, 72-depth planeparallel LTE model atmospheres were computed using the program ATLAS9, written and supplied by Dr. R. L. Kurucz. Assuming that the star would prove to be metal-poor, the model atmospheres were computed using opacity distribution functions and abundances with enhanced abundances of all the " α " elements (O, Ne, Mg, Si, S, Ar, Ca, and Ti) by 0.4 dex. The " α " element enhancements are important since several of these elements are quite abundant and are major electron donors to the H⁻ opacity. During our model

⁶Lee et al. (2001) discussed differential reddening in NGC 6287. Based on the mean turn-off colors in two different pointings of HST NIC3 observations, Lee et al. suggested that $\Delta E(B-V) \approx 0.07 - 0.09$ mag exists across NGC 6287, confirming the previous result of Stetson & West (1994).

computation, the convective overshoot was turned on. This provided our initial model atmospheres for each program star.

The abundance analysis was performed using the programs WIDTH9 (written and supplied by Dr. R. L. Kurucz) and MOOG (Sneden 1973). Adopting the photometric temperature and surface gravity as our initial values, we began by restricting the analysis to those Fe I lines with $\log(W_{\lambda}/\lambda) \leq -5.2$ (i.e. for the linear part of the curve of growth), and comparing the abundances as a function of excitation potential. New model atmospheres were computed with a slightly different effective temperature until the slope of the log n(Fe I) versus χ relation was zero. The stronger Fe I lines were then added and the microturbulent velocity v_{turb} altered until the log n(Fe I) versus $\log(W_{\lambda}/\lambda)$ relation had zero slope. Finally, we analyzed the gravity-sensitive Fe II lines, recomputing new model atmospheres by altering the surface gravity until the iron abundances derived from the Fe I lines agreed with those derived from the Fe II lines.

Table 4 shows comparisons of temperature and surface gravity between the photometric (Alonso et al. 1999) and the spectroscopic methods in our program stars. The temperatures agree well between the two methods, with the exception of NGC 6293-2673. The discrepancy in temperature appears to be related to the interstellar reddening value of the clusters, suggesting that the interstellar reddening values may be slightly incorrect or there exists a differential reddening effect. (It is also likely due in part to the quality of spectra. Our spectra for the NGC 6541 RGB stars are superior to our spectra for the other clusters.) Figure 1 shows the comparisons of our spectroscopic T_{eff} versus photometric and spectroscopic $\log g$ results to those of model isochrones⁷ for [Fe/H] = -2.14 and -1.84, and $[\alpha/Fe] = +0.3$ (Bergbusch & VandenBerg 2001). In the Figure, we also show T_{eff} and $\log g$ of M92 RGB stars (Sneden et al. 1991). The mean metallicity of the M92 RGB stars is $[Fe/H] \approx -2.3$ (Sneden et al. 1991, 2000b) and is more metal-poor than our three program clusters. Our photometric log q results agree well with those of model isochrones, while our spectroscopic $\log g$ results appear to be too small. The disagreement in the surface gravity is rather large and it appears to be related to NLTE effects as suggested by others (see, for example, Nissen et al. 1997; Allendo Prieto et al. 1999). Since metal-poor stars have much weaker metal-absorption in the ultraviolet, more non-local UV flux can penetrate from the deeper layers. This flux is vital in determining the ionization equilibrium of the atoms, resulting in deviations from LTE. Nissen et al. (1997) claimed that surface gravities of metal-poor dwarfs and subgiants derived from the spectroscopic method, which demands that Fe I and Fe II lines should provide the same iron abundance, are a factor of two or three ($\Delta \log q \approx 0.3 - 0.5$)

 $^{^{7}}$ In the Figure, we adopted the model isochrones for 14 Gyr. The age does not significantly affect the RGB loci of the model isochrones with > 10 Gyr.

smaller than those from the Hipparcos parallaxes. Allendo Prieto et al. (1999) also claimed that spectroscopic gravities and those from the Hipparcos parallaxes are in good agreement for stars in the metallicity range $-1.0 < [{\rm Fe/H}] < +0.3$, while large discrepancies can be found for stars with metallicities below $[{\rm Fe/H}] = -1.0$, in the sense that the spectroscopic method provides lower surface gravities. Therefore, we rely on photometric gravities for our abundance analysis. It should be noted that the photometric surface gravity estimate is rather insensitive to the uncertainties in interstellar reddening values. In general, an uncertainty of 0.1 mag in E(B-V) results in an uncertainty of 0.1 dex in the derived photometric surface gravity, in the sense that the photometric surface gravity increases with decreasing E(B-V).

The program MOOG provides a powerful means of synthetic spectrum fitting, which is necessary for the HFS analysis in particular for Ba II lines, for example via the BLENDS driver. To see if there is any systematic difference between the results from WIDTH9 and those from MOOG, we compared the Fe I abundances for NGC 6287-1491 using the same model atmosphere and atomic data and we obtained consistent results between the two, with $\Delta[\log n(\text{Fe I})_{\text{WIDTH9}} - \log n(\text{Fe I})_{\text{MOOG}}] = 0.00 \pm 0.01$. Therefore, we consider that WIDTH9 and MOOG give consistent results to within 0.01 dex and we do not differentiate between the two in the following discussions.

4. RESULTS

4.1. Radial Velocity Measurements

Although radial velocity measurements were not our primary goal, they provide a very useful criterion for cluster membership of the program stars and allow us to update the somewhat uncertain radial velocities of our program clusters. The radial velocity is of particular importance in the kinematic study of inner halo globular clusters. Since there are not yet any proper motion studies of inner halo clusters, the kinematic properties of these clusters have been investigated via statistical analyses using their radial velocities (see, for example, Harris 2001). Previous studies of the radial velocities have been based on low resolution spectra, where the internal measurement error is much larger than ours.

In order to determine the radial velocity, we cross-correlated about 20 orders in our program star spectra with the same orders observed each night for the twilight sky. We show heliocentric radial velocities of individual stars in Table 5. As can be seen in the Table, NGC 6541 I-21 is not a member star of the cluster and we therefore exclude it from our mean velocity calculations. Our mean heliocentric radial velocities for NGC 6287, NGC 6293, and

NGC 6541 are -288.8 ± 3.5 km s⁻¹, -151.9 ± 6.7 km s⁻¹, and -167.5 ± 5.0 km s⁻¹, respectively. (The errors are those of mean.) It should be noted that large uncertainties in our velocity measurements are mainly due to the cluster internal velocity dispersions.

Hesser, Shawl, & Mayer (1986) studied the radial velocities of these three clusters using low resolution image-tube spectrograms, and they obtained $-208 \pm 16 \text{ km s}^{-1}$, $-143 \pm 17 \text{ km s}^{-1}$, $-158 \pm 7 \text{ km s}^{-1}$ for NGC 6287, NGC 6293, and NGC 6541, respectively. Their radial velocities for NGC 6293 and NGC 6541 are in agreement to within the measurement errors. The discrepancy in the radial velocity of NGC 6287, however, is so large that it can not be easily explained by measurement errors. During the 1998 observing run, we obtained a spectrum of HD 166161, whose radial velocity is well known. Using the same procedure described above, we derived $v_r = 68.2 \pm 0.7 \text{ km s}^{-1}$ for HD 166161 and this is in excellent agreement with the previous measurements by others (68.4 \pm 0.3 km s⁻¹, Bond 1980). Therefore, we conclude that our radial velocity measurement for NGC 6287 is correct and differs by almost 80 km s⁻¹ larger than that of Hesser et al. (1986).

Rutledge et al. (1997b) measured the radial velocities for 11 stars in NGC 6541 and obtained a mean radial velocity for the cluster of $v_r = -163.5 \pm 12.4 \text{ km s}^{-1}$. Their radial velocity for NGC 6541 is in good agreement with our value.

4.2. Elemental Abundances and Error Analysis

In Tables 6, 7 and 8, we present the elemental abundances of our program clusters. In the Tables, the elemental abundances using the photometric surface gravities (column $\log g_P$) and the spectroscopic gravities (column $\log g_S$), the uncertainty, and the number of absorption lines used for each element are listed. In both cases, we adopt the spectroscopic temperatures given in Table 4. The [el/Fe] ratios for neutral elements are estimated from [el/H] and [Fe I/H] ratios, with the exception of oxygen. The [el/Fe] for singly ionized elements (Ti II, Ba II, La II, and Eu II) and oxygen are estimated from [el/H] and [Fe II/H] ratios (see, for example, Ivans et al. 2001). The uncertainty quoted is for a single line and, therefore, that of each element is given by σ/\sqrt{n} , where σ is the uncertainty per line and n is the number of absorption lines used for each element. The mean iron abundance [Fe/H]_{avg} is defined to be the unweighted average of [Fe/H]_I and [Fe/H]_{II}. In Table 9, we show the mean results per cluster. It should be noted that we rely on the abundances using the photometric surface gravity and we adopt Fe II abundances for the iron abundances of our program stars since the Fe II abundance is thought to be less sensitive to NLTE conditions (Thévenin & Idiart 1999).

In Table 10, we show estimated errors resulting from uncertainties in the input model atmosphere $\delta T_{eff}=\pm 100~{\rm K},~\delta\log g=\pm 0.3~{\rm and}~\delta v_{turb}=\pm 0.3~{\rm km~s^{-1}},$ which are appropriate for our analysis. In the fourth column of the Table, we also show abundance errors by shifting $\delta T_{eff}=\pm 100~{\rm K}.$ In this case, however, we also alter the photometric $\log g$ and v_{turb} to meet criteria that we used in the previous section [photometric surface gravity and the zero slope in the log n(Fe I) versus $\log (W_{\lambda}/\lambda)$ relation]. The errors in the fourth column have similar values as those in the first column. It should be noted that O, Si, Ba, La, and Eu are very sensitive to T_{eff} resulting in $|\delta[{\rm el/Fe}]/\delta T_{eff}(100~{\rm K})| \approx 0.10-0.14~{\rm dex}.$ Also importantly, the [Si I/Ti I] ratio is very sensitive to T_{eff} . An uncertainty of 100 K in T_{eff} results in $\approx 0.2~{\rm dex}$ in the [Si I/Ti I] ratio. This is mainly due to high sensitivity in the [Ti I/H] ratio to T_{eff} . On the other hand, the [Si I/Ti II] ratio is less sensitive to T_{eff} , $|\delta[{\rm el/Fe}]/\delta T_{eff}(100~{\rm K})| \approx 0.02~{\rm dex}$. Since we are forced to rely on very strong lines, the barium abundance is very sensitive to the microturbulent velocity. Fortunately, the abundance of the other s-process element, lanthanum, relies on weaker lines.

4.3. The α -elements

The measurements of the α -element abundances provide us an opportunity to explore the relative ages of the globular clusters. The enhanced values of these elements in globular clusters are interpreted as the domination by SNe II nucleosynthesis in the proto-stellar material, while lower values are interpreted as due to the increasing contribution of SNe Ia, which are thought to appear 10^9 or more years later (Wyse & Gilmore 1988; Wheeler et al. 1989; Carney 1996).

Carney (1996) suggested that the unweighted mean value of silicon, calcium, and titanium abundances [$\langle \text{Si} + \text{Ca} + \text{Ti} \rangle / \text{Fe}$] is the most representative to the α -element abundance in the globular cluster systems. Since these three elements are not destroyed or produced during the RGB phase, they are less sensitive to the evolutionary effects, such as an internal mixing. We, therefore, define the α -element abundance of the globular clusters to be the unweighted mean value of silicon, calcium, and titanium abundances in the following discussions.

In Figure 2, we show [Si/Fe], [Ca/Fe], [Ti/Fe], and $[\alpha/\text{Fe}]$ of our program clusters along with the "halo" and the "disk" globular clusters⁸ (Gratton 1987; Gratton & Ortolani

 $^{^{8}}$ Zinn (1985) subdivided the globular clusters into the "halo" and the "thick disk" groups at [Fe/H] = -0.8. The halo clusters have an essentially spherical distribution about the Galactic center and they constitute a pressure supported system (a small rotational velocity and a larger velocity dispersion), while the thick disk

1989; Kraft et al. 1992, 1995, 1997, 1998; McWilliam et al. 1992; Sneden et al. 1994, 1997, 2000b; Brown et al. 1997, 1999; Ivans et al. 1999; Shetrone & Keane 2000; Habgood 2001) as a function of [Fe/H]. In Table 11, we summarize the mean α -element abundances of our program clusters and other clusters. It should be noted that we exclude our program clusters from the mean values of the "old halo" globular clusters (OHGCs). In the Table, the errors are those of the mean. The silicon abundances of our program clusters appear to be slightly more enhanced than those of other clusters. On the other hand, the titanium abundances of our program clusters appear to be slightly depleted. The titanium abundance of the metal-poor RGB stars using the neutral titanium lines may suffer from NLTE effects, such as an over-ionization, and the resultant Ti abundance may be spurious. However, our Ti abundance analyses using the Ti II lines also yield lower titanium abundance scales in our program clusters, indicating that they are truly titanium deficient. Note that titanium could be defined partly as an iron-peak element. Explosive nucleosynthesis calculations of the massive stars (Woosley & Weaver 1995) predict that one of the major sources of the SNe II titanium yield is ⁴⁸Cr via the consecutive electron capture processes.

4.4. The Heavy Neutron Capture Elements Ba, La, and Eu

In Figure 4, we show Ba, La, and Eu abundances of the globular clusters (Gratton et al. 1986; Gratton 1987; Gratton & Ortolani 1989; McWilliam et al. 1992; Brown et al. 1997, 1999; Sneden et al. 1997; Kraft et al. 1998; Ivans et al. 1999; Shetrone & Keane 2000; Sneden et al. 2000a, 2000b) and field stars (Burris et al. 2000) as a function of metallicity. In Figure 5, we show [Ba/Eu], and [La/Eu] ratios as a function of [Fe/H]. The Figures suggest that the s-process elements La and Ba are slightly more enhanced in our program clusters than in the field stars. Figure 6 shows the elemental abundances of Ba, La, and Eu of our

clusters have a highly flattened spatial distribution and constitute a rotational supported system (a larger rotational velocity and a smaller velocity dispersion). Searle & Zinn (1978) and Lee, Demarque, & Zinn (1994) suggested that the inner halo globular clusters exhibit a tight HB morphology versus [Fe/H] relation, while the outer halo globular clusters show the second parameter phenomenon (i.e., a larger scatter in HB type at a given [Fe/H]). Subsequently, Zinn (1993) subdivided the halo clusters into two groups. The "old halo" group obeys the same HB type versus [Fe/H] relationship as the inner halo clusters while the "younger halo" group deviates from this relationship by a significant amount (see Figure 3). Zinn (1993) and Da Costa & Armandroff (1995) argued that the old and the younger halo groups have different kinematic properties that the old halo group has a prograde mean rotation velocity with a smaller velocity dispersion while the younger halo group has a retrograde mean rotation velocity about the Galactic center with a larger velocity dispersion. They suggested that the old halo group formed during the collapse that led ultimately to the formation of the Galactic disk and the younger halo group were accreted later in time.

program clusters and M15 (Sneden et al. 2000a). We also plot the solar abundances of the neutron capture elements with $56 \le Z \le 64$, those due to the r- and s-process contributions (Burris 2000). In the Figure, these elemental abundances were normalized to the r-process element europium. As suggested by others (Cowan et al. 1999; Burris et al. 2000; Sneden et al. 2000a), the solar neutron capture element distribution due to the r-process contribution is consistent with those of M15 within the measurement error. However, the s-process elements Ba and La in our program clusters appear to be slightly enhanced, consistent with Figure 5. This enhanced s-process element distribution of the inner halo globular clusters may suggest that they might have experienced a different chemical enrichment history than other halo globular clusters or the metal-poor field stars.

5. THE CHEMICAL EVOLUTION OF THE INNER HALO GLOBULAR CLUSTERS

As Zinn (1993) and Da Costa & Armandroff (1995) suggested, if the bulk of "younger halo" globular clusters (YHGCs) were accreted into our Galactic halo after the formation of the OHGCs, elemental abundance patterns in YHGCs may not fully reflect the chemical evolution history of our Galactic halo, since YHGCs could have experienced very different chemical evolution history than OHGCs. Also the number of YHGCs studied employing high-resolution spectroscopy is too small as yet to delineate their chemical evolution history. Therefore, we focus on OHGCs in our following discussions.

Figure 7 shows [Si/Fe], [Ca/Fe], [Ti/Fe], [α /Fe], and [Fe/H] ratios of the OHGCs as a function of their current Galactocentric distance R_{GC} . In the Figure, the [Si/Fe] ratios of the OHGCs appear to decrease with the Galactocentric distance, while the [Ti/Fe] ratios increase with the Galactocentric distance, although the gradient in [Ti/Fe] versus R_{GC} is rather marginal. [Ca/Fe] and [α /Fe] ratios appear to remain constant ($\approx +0.30$) with the Galactocentric distance. It is thought that the variations in [Si/Fe] and [Ti/Fe] ratios with the Galactocentric distance cancel each other, providing constant [α /Fe] ratios with the Galactocentric distance. The [Fe/H] values of OHGCs show a large scatter around the mean value ([Fe/H] ≈ -1.6), however, the absence of gradient in [Fe/H] versus R_{GC} suggests that sampling different metallicity OHGCs as a function of R_{GC} is not responsible for the gradients in [Si/Fe] and [Ti/Fe] ratios with R_{GC} .

In Figure 8, we show the [Si/Ti] ratios of the OHGCs as a function of their Galactocentric distance. In the Figure, we also show the least-square fit, the inverse least-square fit, and the bisector liner fit (Isobe et al. 1990) to the data. Our slope of the bisector linear fit to the data is δ [Si/Ti]/ δ log $R_{GC} = -0.765$ dex per decade. We performed a non-parametric Spearman

rank-order test (Press et al. 1992) and our results indicate a probability of ≈ 0.7 % that the anti-correlation between [Si/Ti] and R_{GC} of the OHGCs is random. In the Figure, we also show the bisector linear fit to the OHGCs with $R_{GC} \leq 8$ kpc (12 clusters) and we found the slope of δ [Si/Ti]/ δ log $R_{GC} = -0.976$ dex per decade. We also performed a Spearman rank-order test and we obtain a probability of ≈ 0.0003 % that the anti-correlation between [Si/Ti] and R_{GC} of the OHGCs with $R_{GC} \leq 8$ kpc is random.

Figure 7 and 8 suggest that the silicon and titanium abundances of the OHGCs are related to their current Galactocentric distances. To explain these elemental abundance gradients, we show the SNe II yields as a function of a progenitor mass with $Z=10^{-4}$ in Figure 9 (Woosley & Weaver 1995). For massive SNe II models, we adopt the U30B, U35B, and U40B models of Woosley & Weaver (1995) following Timmes, Woosley, & Weaver (1995). Since Woosley & Weaver (1995) provided ejected masses of the individual isotopes from 1 H to 71 Ge at 2.5×10^{4} seconds after the explosion in their Tables 14A and 14B, we need to consider the radioactive decays, such as negative beta decay and electron capture, of the short- and intermediate-lived radioactive isotopes to derive the final products by the SNe II explosion. In the inset of the Figure, we also show the SNe Ia yields by Höeflich, Wheeler, & Thielemann (1998). Note that SNe yields are given in units of solar masses and not in [el/H] and the abscissa of the inset is the atomic number.

As shown in Figure 9, the chemical enrichment by the massive SNe II explosion will lead to elemental abundance anomalies, in the sense that [O/Fe] and [Si/Fe] ratios will increase, while [Ti/Fe] ratios¹⁰ will decrease. We suggest that the gradient in the [Si/Ti] ratios versus R_{GC} can be explained by the contributions from the SNe II explosions with the different progenitors' masses. Due to its deeper gravitational potential and the denser environment, the central regions of our Galaxy would have been better able to retain the ejecta from massive SNe II explosions that have higher specific kinetic energies compared to the intermediate or the outer halo. Although weak, the enhanced [O/Fe] ratios of the NGC 6287 RGB stars with $[Na/Fe] \geq 0.0$ may support this scenario (see also Matteucci & Greggio 1986), since the original [O/Fe] ratios would have been much higher than the

⁹It should be noted that the difference in the [Si/Ti] ratios that we found may be due, in part, to different methods of analyses and that a thorough re-analysis of all the data using the same analysis techniques may be very useful. Also importantly, using $[Si\ I/Ti\ II]$ ratios to investigate the [Si/Ti] versus R_{GC} anti-correlation would be very desirable, since $[Si\ I/Ti\ II]$ ratios are not sensitive to the uncertainties in the input model atmosphere as we discussed above. Unfortunately, most of titanium abundances of the OHGCs that we adopted from the literature rely on Ti I lines.

¹⁰It should be noted that the SNe II titanium yields of Woosley & Weaver (1995) are too low to explain observed titanium abundances (Timmes, Woosley, & Weaver 1995).

observed ratios if a substantial amount of oxygen atoms had been already destroyed via the deep mixing scenario (see, for example, Kraft 1994). As we have already mentioned, the major contributor to the titanium abundance due to the SNe II explosion is 48 Cr, which decays into 48 Ti. Nakamura et al. (1999) argued that the SNe II Cr yields will decrease as the mass of the progenitor increases, leading to decreasing [Cr/Fe] ratios toward lower [Fe/H]. Thus, the behavior of observed [Cr/Fe] ratios in the metal-poor field stars may support the argument that more massive SNe II may have contributed to the early nucleosynthesis in our Galaxy. SNe Ia explosion models also predict that a significant amount of silicon can be produced by SNe Ia explosions (see Figure 9; see also Nomoto, Thielemann, & Yokoi 1984), however, the chemical enrichment by SNe Ia explosions is not likely responsible for the gradient in [Si/Ti] ratios versus R_{GC} . The OHGCs are very old to within 0.5 - 1.0 Gyr (see, for example, Rosenberg et al. 1999; Lee et al. 2001; Lee, Carney, & Heasley 2002, in preparation) and SNe Ia contributions begin to appear at least 1 - 2 Gyr after star formation is initiated.

On the other hand, our measurements of s-process¹¹ elements Ba and La may indicate that they formed in PGCCs which had already been polluted by low- or intermediate-mass AGB stars, unless the observed Ba and La were produced internally and dredged-up to the stellar surface, and may provide an additional constraint on the formation epoch of our program clusters. If the s-process site is intermediate mass AGB stars, which should begin to appear about 10^8 yr after star formation initiated (Matteucci 2002), the formation timescale of our program clusters might be as short as a few times 10^8 yr after the star formation is initiated in the Galaxy's central regions.

Perhaps a similar situation can be found in the recent study of Ivans et al. (2001), Fulbright (2001), and Stephens & Boesgaard (2002). Ivans et al. (2001) compared the intermediate metallicity clusters M4 ([Fe/H] = -1.08) and M5 ([Fe/H] = -1.21) and they suggested that Si, Ba and La are overabundant in M4 with respect to those in M5. It should be noted that apogalacticon distances of the clusters are ≈ 6 kpc for M4 and ≈ 40 kpc for M5 (Dinescu et al. 1999). Fulbright (2001) performed an abundance study of metal poor field stars and discussed their kinematics versus elemental abundance relationships. He suggested that the lower velocity stars (mean $R_{max} = 9.1$ kpc and $|Z_{max}| = 0.6$ kpc) in the solar neighborhood appear to have higher [Si/Fe] and [Ba/Eu] ratios than the highest velocity stars (mean $R_{max} = 37.4$ kpc and $|Z_{max}| = 6.2$ kpc). Finally, Stetphens & Boesgaard (2002) studied elemental abundances of the kinematically peculiar field halo stars and they argued that $[\alpha/Fe]$ ratios are anticorrelated with apogalacticon distances R_{apo} .

¹¹In the metal-poor field stars, contributions from the s-process can first be seen in metallicities as low as $[Fe/H] \approx -2.75$ (Burris et al. 2000).

On the other hand, the opposite situation can be found in the Galactic bulge stars studied by McWilliam & Rich (1994). They analyzed the chemical abundances of a dozen metal-rich K giants in the Galactic bulge and found that [Mg/Fe] and [Ti/Fe] are enhanced by ≈ 0.3 dex, while [Ca/Fe] and [Si/Fe] are depleted by ≈ 0.2 dex. As we discussed above, the oxygen abundances in RGB stars are hard to determine, due to internal mixing during the RGB phase, which depletes the oxygen abundance in the stellar photosphere. The anticorrelation of sodium and oxygen abundances is a good means by which we may estimate if an individual red giant has experienced significant mixing or not (Kraft 1994). In particular, low sodium abundances ($[Na/Fe] \le 0$) appears to be a good indicator of minimal mixing in red giants. The two stars in McWilliam & Rich (1994) with $[Na/Fe] \leq 0.0$ have a mean [O/Fe] value of $+0.05 \pm 0.05$, consistent with their result $[O/Fe] \approx 0.0$. They also found that the r-process element Eu appears to be enhanced, while the iron-peak elements and s-process elements appear to be normal relative to Fe. Our results and those of McWilliam & Rich (1994) may reflect a complexity of the chemical enrichment history near the Galactic center so that one can hardly draw a boundary between the SNe II contribution and that due to the SNe Ia events. Perhaps a comparison between our results and those of McWilliam & Rich (1994) might be rather inappropriate since the ages of bulge giants are not known but presumably they are younger than our program clusters. During the formation time lag between our program clusters and bulge giants, the proto-bulge star clouds must have been polluted by the nucleosynthesis in the Galaxy's central regions and, in particular, by infalling gas. 12 Therefore, the one-to-one elemental abundance comparison between our program clusters and bulge giants to trace the chemical enrichment history of our Galaxy's central regions may be difficult.

6. SUMMARY AND CONCLUSIONS

A chemical abundance study of the old inner halo clusters NGC 6287, NGC 6293, and NGC 6541 has been presented. Our metallicity estimates for NGC 6287, NGC 6293, and NGC 6541 are $[Fe/H] = -2.01 \pm 0.05$, -1.99 ± 0.02 , and -1.76 ± 0.02 (internal), respectively, and our metallicity measurements are in good agreement with previous estimates.

Our radial velocity measurements for NGC 6293 and NGC 6541 are in good agreement with those by Hesser et al. (1986) and Rutledge et al. (1997b), but our radial velocity

 $^{^{12}}$ Matteucci (2002, see also references therein) suggested that a fast accumulation of gas in the Galaxy's central regions accompanied by fast star formation is the best scenario to reproduce the bulge stars' elemental abundance distribution.

measurement for NGC 6287 is almost 80 km $\rm s^{-1}$ larger than that of Hesser et al. (1986).

We have discussed that the mean α -element abundances ([$\langle Si + Ca + Ti \rangle / Fe$]) of our program clusters are in good agreement with other globular clusters, $[\alpha/\text{Fe}] \approx +0.3$, confirming the previous results of Carnev (1996). However, the individual α -elements appear to follow different trends. The silicon abundances of the inner halo clusters appear to be enhanced and the titanium abundances appear to be depleted compared to the intermediate halo clusters. In particular, the [Si/Ti] ratios of OHGCs appear to be related to their Galactocentric distances, in the sense that the [Si/Ti] ratios decrease with Galactocentric distance. We proposed that contributions from different masses of the SNe II progenitors that exploded before the formation of OHGCs and the different initial physical environments surrounding the PGCCs are responsible for this gradient in [Si/Ti] ratios versus Galactocentric distances of OHGCs. The high [Si/Ti] ratios toward the Galactic center may be due to a higher proportion of high-mass SNe II contributions to the PGCCs. On the other hand, our program clusters appear have enhanced s-process elemental abundances, providing an additional constraint on the formation epoch of our program clusters. If the s-process site is intermediate mass AGB stars, which should begin to appear about 10⁸ yr after star formation is initiated, the formation timescale of our program clusters might be as short as a few times 10^8 yr.

In the future, it would be very desirable to investigate the α -element abundances and the neutron capture elemental abundances of the inner halo or bulge clusters with an expanded sample, and preferentially at shorter wavelengths where more neutron capture elements' absorption lines are found.

This is part of Ph.D. thesis work of J. -W. Lee at the University of North Carolina at Chapel Hill. J. -W. Lee thanks Chris Sneden, Jim Rose, Art Champagne, Luisa de Almeida, Mike Habgood, and Inese Ivans for their kind discussions and Young-Wook Lee and Suk-Jin Yoon for providing recent HB isochrones. We also thank the anonymous referee for a thorough and beneficial review. This research was supported by the National Aeronautics and Space Administration (NASA) grant number GO-07318.04-96A from the Space Telescope Science Institute, which is operated by the Association of Universities for Research in Astronomy (AURA), Inc., under NASA contract NAS 5-26555 and the National Science Foundation grants AST96-19381 and AST99-88156. Support for this work was also provided in part by the Creative Research Initiative Program of Korean Ministry of Science and Technology.

REFERENCES

Alcaino, G. 1979, A&AS, 35, 233

Allendo Prieto, C., Garcia López, R., Lambert, D. L., & Gustafsson, B. 1999, ApJ, 527, 879

Alonso, A., Arribas, S., & Martinez-Roger, C. 1999, A&AS, 140, 261

Bard, A., Kock, A., & Kock, M. 1991, A&A, 248, 315

Bard, A., & Kock, M. 1994, A&A, 282, 1014

Bergbusch, P. A., & VandenBerg, D. A. 2001, ApJ, 556, 322

Biémont, E., Baudous, M., Kurucz, R. L., Ansbacher, W., & Pinnington, E. H. 1991, A&A, 249, 539

Biémont, E., Karner, C., Meyer, G., Traeger, F., & Zu Putlitz, G. 1982, A&A, 107, 166

Blackwell, D. E., Booth, A. J., Haddock, D. J., Petford, A. D., & Leggett, S. K., 1986a, MNRAS, 220, 549

Blackwell, D. E., Booth, A. J., Menon, S. L. R., & Petford, A. D. 1986b, MNRAS, 220, 289

Blackwell, D. E., Menon, S. L. R. & Petford, A. D. 1983, MNRAS, 204, 883

Blackwell, D. E., Menon, S. L. R., Petford, A. D., & Shallis, M. J. 1982a, MNRAS, 201, 611

Blackwell, D. E., Petford, A. D., & Shallis, M. J. 1979, MNRAS, 186, 657

Blackwell, D. E., Petford, A. D., Shallis, M. J., & Simmons, G. J. 1982b, MNRAS, 199, 43

Blackwell, D. E., Petford, A. D., & Simmons, G. J. 1982c, MNRAS, 201, 595

Blackwell, D. E., Smith, G., & Lynas-Gray, A. E. 1995, A&A, 303, 575

Bond, H. E. 1980, ApJS, 44, 517

Brown, J. A., Wallerstein, G., & Gonzalez, G. 1999, AJ, 118, 1245

Brown, J. A., Wallerstein, G., & Zucker, D. 1997, AJ, 114, 180

Burris, D. L., Pilachowski, C. A., Armandroff, T. E., Sneden, C., Cowan, J. J., & Roe, H. 2000, ApJ, 544, 302

Cardon, B. L., Smith, P. L., Scalo, J. M., & Testerman, L. 1982, ApJ, 260, 395

Carney, B. W. 1996 PASP, 108, 900

Cowan, J. J., Pfeiffer, B., Kratz, K. L., Thielemann, F. K., Sneden, C., Burles, S., Tytler, D., & Beers, T. C. 1999, ApJ, 521, 194

Da Costa, G. S., & Armandroff, T. E. 1995, AJ, 109, 2533

Dinescu, D. I., Girard, T. M., & van Altena, W. F. 1999, AJ, 117, 1792

- Fulbright, J. P. 2001, AJ, 123, 404
- Fuhr, J. R., Martin, G. A., & Wiese, W. L. 1998a, Atomic transition probabilities. Scandium through Manganese, Vol. 17 No. 3 (New York: American Institute of Physics and American Chemical Society)
- Fuhr, J. R., Martin, G. A., & Wiese, W. L. 1998b, Atomic transition probabilities. Iron through Nickel, Vol. 17 No. 4 (New York: American Institute of Physics and American Chemical Society)

Garz, T. 1973, A&A, 26, 471

Geisler, D. 1988, PASP, 100, 687

Gratton, R. G. 1987, A&A, 179, 181

Gratton, R. G., & Ortolani, S. 1989, A&A, 211, 41

Gratton, R. G., Quarta, M. L., & Ortolani, S. 1986, A&A, 169, 208

Grevesse, N., Blackwell, D. E., & Petford, A. D. 1989, A&A, 208, 157

Habgood, M. J. 2001, PhD thesis, The University of North Carolina at Chapel Hill

Harris, W. E. 1996, AJ, 112, 1487

Harris, W. E. 2001, in Star Clusters: Proceedings of the 28th Advanced Course of the Swiss Society of Astronomy and Astrophysics (Observatoire de Genève: Switzerland)

Hesser, J. E., Shawl, S. J., & Meyer, J. E. 1986, PASP, 98, 403

Höeflich, P., Wheeler, J. C., & Thielemann, F. K. 1998, ApJ, 495, 617

Isobe, T., Feigelson, E. D., Akritas, M. G., & Babu, G. J. 1990, ApJ, 364, 104

Ivans, I. I., Kraft, R. P., Sneden, C., Smith, G. H., Rich, R. M., & Shetrone M. 2001, AJ, 122, 1438

Ivans, I. I., Sneden, C., Kraft, R. P., Suntzeff, N. B., Smith, V. V., Langer, G. E., & Fulbright, J. P. 1999, AJ, 118, 1273

Janes, K. A., & Heasley, J. N. 1991, AJ, 101, 2097

Kennedy, D. C., Bates, B., & Kemp, S. N. 1998, A&A, 336, 315

Kraft, R. P. 1994, PASP, 106, 553

Kraft, R. P., Sneden, C., Langer, G. E., & Prosser, C. F. 1992, AJ, 104, 645

Kraft, R. P., Sneden, C., Langer, G. E., Shertrone, M. D., & Bolte, M. 1995, AJ, 109, 2586

Kraft, R. P., Sneden, C., Smith, G. H., Shertrone, M. D., & Fulbright, J. 1998, AJ, 115, 1500

Kraft, R. P., Sneden, C., Smith, G. H., Shertrone, M. D., Langer, G. E., & Pilachowski, C. A. 1997, AJ, 113, 279

Kurucz R. L. 1995, CD-ROM No.23

Lambert, D. L. 1978, MNRAS, 182, 249

Lee, J.-W., Carney, B. W., Fullton, L. K., & Stetson, P. B. 2001, AJ, 122, 3136

Lee, Y.-W, Demarque, P., & Zinn, R. 1994, ApJ, 423, 248

Livingston, C. W. 1999, in Allen's Astrophysical Quantities (Fourth Edition), p. 339

Matteucci, F. 2002, astro-ph/0203340

Matteucci, F., & Greggio, L. 1986, A&A, 154, 279

McWilliam, A. 1998, AJ, 115, 1640

McWilliam, A., Geisler, D., & Rich, R. M. 1992, PASP, 104, 1193

McWilliam, A., & Rich, R. M. 1994, ApJS, 91, 749

Nakamura, T., Umeda, H., Nomoto, K., Thielemann, F., & Burrows, A. 1999, ApJ, 517, 193

Nissen, P. E., Hoeg, E., & Schuster, W. J. 1997, ESA SP-402: Hipparcos - Venice 97, 402, 225

Nomoto, K., Thielemann, F. K., & Yokoi, K. 1984, ApJ, 286, 644

O'Brian, T. R., Wickliffe, M. E., Lawler, J. E., Whaling, W., & Brault, J. W. 1991, J. Optical Soc. America, B8, 1185

Press, W. H., Teukolsky, S. A., Vetterling, W. T., & Flannery, B. P. 1992, Numerical Recipes (Cambridge: Cambridge Univ. press)

Prochaska, J. X., Naumov, S. O., Carney, B. W., McWilliam, A., & Wolfe, A. M. 2000, AJ, 120, 2513

Rey, S.-C., Yoon, S.-J., Lee, Y.-W., Cahboyer, B., & Sarajedini, A. 2001, AJ, 122, 3219

Rosenberg, A., Saviane, I., Piotto, G., & Aparicio, A. 1999, AJ, 118, 2306

Rutledge, G. A., Hesser, J. E., & Stetson, P. B. 1997a, PASP, 109, 907

Rutledge, G. A., Hesser, J. E., Stetson, P. B., Mateo, M., Simard, L., Bolte, M., Friel, E. D., & Copin, Y. 1997b, PASP, 109, 883

Searle, L., & Zinn, R. 1978, ApJ, 225, 357

Shetrone, M. D., & Keane, M. J. 2000, AJ, 119, 840

Smith, G. 1981, A&A, 103, 351

Sneden, C. 1973, PhD thesis, The University of Texas at Austin

Sneden, C., Johnson, J., Kraft, R. P., Smith, G. H., Cowan, J. J. & Bolte, M. S. 2000a, ApJ, 536, L85

Sneden, C., Kraft, R. P., Langer, G. E., Prosser, C. F. & Shetrone, M. D. 1994, AJ, 107, 1773

Sneden, C., Kraft, R. P., Prosser, C. F., & Langer, G. E. 1991, AJ, 102, 2001

Sneden, C., Kraft, R. P., Shetrone, M. D., Smith, G. H., Langer, G. E., & Prosser, C. F. 1997, AJ, 114, 1964

Sneden, C., Pilachowski, C. A., & Kraft, R. P. 2000b, AJ, 120, 1351

Stephens, A., & Boesgaard, A. M. 2002, AJ, 123, 1647

Stetson, P. B., & West, M. J. 1994, PASP, 106, 726

Thévenin, F. 1990, A&AS, 82, 179

Thévenin, F., & Idiart, T. P. 1999, ApJ, 521, 753

Timmes, F. X., Woosley, S. E., & Weaver, T. A. 1995, ApJS, 98, 617

Whaling, W., Hannaford, P., Lowe, R. M., Biémont, E., & Grevesse, N. 1985, A&A, 153, 109

Wheeler, J. C., Sneden, C., & Truran, J. W. 1989, ARA&A, 27, 279

Woosley, S. E., & Weaver, T. A. 1995, ApJS, 101, 181

Wyse, R. F. G., & Gilmore, G. 1998, AJ, 95, 1404

Zinn, R. 1985, ApJ, 293, 424

Zinn, R. 1993, in The Globular Cluster-Galaxy Connection, ASP Conf. Ser. Vol. 48, edited by G. H. Smith and J. P. Brodie (A.S.P., San Francisco), p. 38

Zinn, R., & West, M. J. 1984, ApJS, 55, 45

This preprint was prepared with the AAS LATEX macros v5.0.

Table 1. Journal of observations.

Id.		V	B-V	Date/Time (UT Start)	t_{exp} (sec)	S/N (total S/N)	Note
NGC 6287	1491	14.22	1.68	1998 Jun 18 23:24	3600	45	
				1998 Jun 19 00:29	3600	45	
				1998 Jun 19 01:31	3600	50	
				1998 Jun 19 02:32	3600	50	$S/N \approx 95$
	1387	14.28	1.87	1998 Jun 20 04:21	3600	45	
				1998 Jun 22 03:12	3000	40	
				1998 Jun 22 04:07	3000	25	
				1999 Jul 05 03:22	2400	50	
				1999 Jul 05 04:04	2400	55	$S/N \approx 95$
	1191	14.58	1.64	1999 Jul 05 02:26	3000	40	
NGC 6293	2673	13.46	1.53	1998 Jun 21 23:10	2400	55	
				1998 Jun 21 23:55	3600	50	
				1998 Jun 22 00:59	3600	50	
				1998 Jun 22 02:02	3600	50	$S/N \approx 100$
	3857	14.11	1.49	1999 Jul 06 02:46	2400	35	•
				1999 Jul 06 03:29	3000	35	
				1999 Jul 06 04:21	3000	45	
				1999 Jul 06 05:14	3000	45	
				1999 Jul 06 06:07	3000	50	$S/N \approx 95$
NGC 6541	I-44	12.54	1.34	1999 Jul 04 01:40	2400	80	
				1999 Jul 04 02:26	2400	80	
				1999 Jul 04 03:07	2400	80	$S/N \approx 135$
	II-113	12.55	1.39	1999 Jul 05 04:51	2400	80	,
				1999 Jul 05 05:33	2400	85	
				1999 Jul 05 06:14	2400	80	$S/N \approx 140$
	I-21	12.46	1.31	1998 Jun 21 04:45	2400	70	Non Member
				1998 Jun 21 05:30	2400	60	
				1998 Jun 21 06:14	2400	60	$\mathrm{S/N}\approx110$

Table 2. Equivalent widths.

λ (Å)	Elem.	χ (eV)	$\log gf$	Ref.		NGC 628			6293		C 6541
					1491	1387	1191	2673	3857	I-44	II-113
6300.23	[O I]	0.00	-9.750	1	24	27	18		8	7	21
6363.88	[O I]	0.02	-10.250	1	8	9					8
5682.63	Na I	2.10	-0.890	2	16	45		31			
5688.22	Na I	2.10	-0.580	2				51			
6154.23	Na I	2.10	-1.560	3		13				13	10
6160.75	Na I	2.10	-1.260	3		24		16	8	23	21
5711.10	Mg I	4.34	-1.750	4	33	52		16	23		67
7387.69	Mg I	5.75	-1.200	4		7					10
6696.03	Al I	3.14	-1.570	5		16		19	12	54	38
6698.67	Al I	3.14	-1.890	5		8		11			21
5665.56	Si I	4.92	-2.040	6	8			12			
5690.43	Si I	4.93	-1.870	6	12	14		17			
5701.10	Si I	4.93	-2.050	6		13					
5708.40	Si I	4.95	-1.470	6		22		27			
5772.15	Si I	5.08	-1.750	6				16	10	21	19
5948.55	Si I	5.08	-1.230	6		30		34	21	40	44
7034.90	Si I	5.87	-0.880	6		10		11		17	20
7405.77	Si I	5.61	-0.820	6		20				36	43
5588.75	Ca I	2.53	0.358	7	88	105					
5590.11	Ca I	2.52	-0.571	7	37	48		51			
5594.46	Ca I	2.52	0.097	7	83	83		99			
5857.45	Ca I	2.93	0.240	7	61	72	58	82	57	99	103
6161.30	Ca I	2.52	-1.266	7	18	18		28	13	42	45
6166.44	Ca I	2.52	-1.142	7	18	22		21	21		47
6169.04	Ca I	2.52	-0.797	7	35	46		52	34		
6169.56	Ca I	2.53	-0.478	7	48	58		62	42	83	91
6439.08	Ca I	2.53	0.390	7	115	126	96		98		146
6449.81	Ca I	2.52	-0.502	7	54	62	48	68	47	84	
6455.60	Ca I	2.52	-0.302 -1.290	7	14	20		20	12	40	40
6471.66	Ca I	2.53	-0.686	7	44	47	37	48	43	78	88
6493.78	Са I	2.52	-0.109	7	83	91		87	64	114	118
6499.65	Ca I	$\frac{2.52}{2.52}$	-0.109 -0.818	7	31	48	35	39	32	71	79
6717.68	Ca I	$\frac{2.52}{2.71}$	-0.513 -0.524	7	48		29	52	37	80	91
7148.15	Ca I	$\frac{2.71}{2.71}$	-0.524 0.137	7	89	104	$\frac{29}{72}$		73		134
7202.20	Ca I	$\frac{2.71}{2.71}$	-0.137 -0.262	7	65	68		69	50	105	103
5866.45	Ti I	1.07	-0.202 -0.784	8	34	42		51		74	77
5880.31	Ti I	1.07	-0.784 -1.989	9						13	15
5899.30	Ti I		-1.989 -1.098		29	29					
	Ti I	1.05		8 9							47
5922.11		1.05	-1.410								
5953.16	Ti I	1.89	-0.273	10	14	16	• • •	20	10	43	37
5965.83	Ti I	1.88	-0.353	10	14	12	• • •	• • •	• • •	38	37
6064.63	Ti I	1.05	-1.888	9	•••	• • •	• • •	• • • •	• • •	20	20
6091.18	Ti I	2.30	-0.413	10	17		• • •	• • • •	• • •	10	14
6126.22	Ti I	1.07	-1.369	9	17	20	• • •		10	41	44
6258.11	Ti I	1.44	-0.299	10	37	46	• • • •	39	10	71	• • •
6258.71	Ti I	1.46	-0.270	10	40	43	• • •	56	23	87	• • •
6261.11	Ti I	1.43	-0.423	10	29	41	• • •	• • •	30	71	
6312.24	Ti I	1.46	-1.496	10	• • • •	• • •	• • •		• • •	13	11

Table 2—Continued

λ (Å)	Elem.	χ (eV)	$\log gf$	Ref.	1	NGC 628	7		6293	NGC 6541	
					1491	1387	1191	2673	3857	I-44	II-113
6336.10	Ti I	1.44	-1.687	10						10	
6554.22	Ti I	1.44	-1.162	10						25	
6556.06	Ti I	1.46	-1.018	10							34
6599.13	Ti I	0.90	-2.029	9		10				19	25
7357.74	Ti I	1.44	-1.066	10						36	43
6606.95	Ti II	2.06	-2.790	11	8	8			9	16	15
7214.74	Ti II	2.59	-1.740	11	16	18		18	12	33	29
5698.52	VI	1.06	-0.111	12				18			
5703.58	VI	1.05	-0.212	12				17	18		
5727.58	VI	1.08	-0.012	12						47	51
5731.25	VI	1.06	-0.730	12						11	13
6081.44	VI	1.05	-0.579	12				10	8	15	26
6090.22	VI	1.08	-0.062	12	17	24		23		45	44
6111.65	VI	1.04	-0.715	12						15	17
6119.53	VI	1.04	-0.713 -0.320	12				13		32	31
6135.36	VI	1.05	-0.320 -0.746	12						14	17
6251.82	VI	0.29	-0.740 -1.342	12	12			15		34	36
6274.65	VI	0.29 0.27	-1.673	12		11				16	
	VI	0.27	-1.510	12						23	
6285.15 6292.82	VI	0.28 0.29		$\frac{12}{12}$						23 26	$\frac{28}{33}$
			-1.471		• • • •			14			
6296.49	VI	0.30	-1.590	12		• • •	• • •	• • •	• • •	27	31
5783.89	Cr I	3.32	-0.295	11	• • • •	• • •	• • •	• • •	• • •	18	
6978.49	Cr I	3.46	0.142	11			• • •			• • •	22
7355.93	Cr I	2.89	-0.285	11	12	18	• • •	16	11		38
7400.23	Cr I	2.90	-0.111	11	18	28	• • •	24	15	66	51
5569.62	Fe I	3.42	-0.544	19	82		• • •	100	• • •	• • • •	• • • •
5586.76	Fe I	3.37	-0.161	17		123	• • •	117	• • •		• • •
5701.55	Fe I	2.56	-2.216	15	53	76	• • •	65	• • •	• • • •	
5705.47	Fe I	4.30	-1.421	19	• • •	• • •	• • •	9	• • •	11	12
5753.12	Fe I	4.26	-0.705	17	19	26	• • •	30	19	43	48
5775.08	Fe I	4.22	-1.314	17	11	11	• • •	12	10	27	26
5778.45	Fe I	2.59	-3.475	19	• • •	14	• • • •	11	• • •	16	21
5909.97	Fe I	3.21	-2.643	19	9	• • •		• • • •	• • •	26	• • •
5916.25	Fe I	2.45	-2.994	14	24	48	22	39	20	65	62
5956.69	Fe I	0.86	-4.608	16	65	84	36	81	47	93	106
6027.05	Fe I	4.08	-1.106	17	15	27	16	19	18	37	41
6065.48	Fe I	2.61	-1.530	15	105	112	86	114	94	132	136
6082.71	Fe I	2.22	-3.573	14	13	21	11	25	12	43	42
6137.69	Fe I	2.59	-1.403	15	108	134	• • •	130	97	• • •	• • •
6151.62	Fe I	2.18	-3.299	14	29	47	30	48	32	65	68
6165.36	Fe I	4.14	-1.490	17	11	12	• • •	11		18	15
6173.34	Fe I	2.22	-2.880	14	52	65	38	61	42	93	90
6200.31	Fe I	2.61	-2.437	15	54	64	33	57	38	81	84
6219.28	Fe I	2.20	-2.433	14	87	101	65	104	75	114	106
6229.23	Fe I	2.85	-2.846	18	12	17	11	16	14	35	35
6230.73	Fe I	2.56	-1.281	15	116	150		155	109		
6232.64	Fe I	3.65	-1.283	19	34	41	28	38	27	57	61
6240.64	Fe I	2.22	-3.190	18	35	41		39	20	65	63

Table 2—Continued

λ (Å)	Elem.	χ (eV)	$\log gf$	Ref.	1	NGC 628	7	NGC	6293	NGC 6541		
					1491	1387	1191	2673	3857	I-44	II-113	
6246.32	Fe I	3.60	-0.894	18	65	66	41	67	56	94	95	
6252.55	Fe I	2.40	-1.687	14	111	119	93	129	92	138	143	
6265.13	Fe I	2.18	-2.550	14	72	96	73	97	73	112	116	
6270.22	Fe I	2.86	-2.505	18	34	29		28	22	53	52	
6280.63	Fe I	0.86	-4.390	16	76	108		106	70			
6297.79	Fe I	2.22	-2.740	14	56	81	50	78	42	96	104	
6301.50	Fe I	3.65	-0.766	18	65		54	71	59	89	97	
6322.69	Fe I	2.59	-2.426	15	50	67	38	66	36		85	
6335.33	Fe I	2.20	-2.194	17		110	80	114	85	129	130	
6336.82	Fe I	3.69	-0.916	19	54	62	37	59	40	87	85	
6344.15	Fe I	2.43	-2.923	14	41	50	38	56	27	79	71	
6358.69	Fe I	0.86	-4.468	13	78	109		101	60			
6393.60	Fe I	2.43	-1.469	18	120	135		144	119	153	151	
6408.02	Fe I	3.69	-1.066	18	41	51	35	50	34	72	77	
6411.65	Fe I	3.65	-0.734	18	65	82	57	77	53		100	
6421.35	Fe I	2.28	-2.027	14	101	120		123	85			
6430.84	Fe I	2.18	-2.006	14	113	134	104	137	102	138	148	
6481.87	Fe I	2.28	-2.984	14	42	62	46	56	33	78	80	
6494.98	Fe I	2.40	-1.273	14	137	158	121	162	129	173	188	
6498.95	Fe I	0.96	-4.687	16	56	71		77	39			
6574.23	Fe I	0.99	-5.004	16	35	41	22	52	26	59	74	
6581.21	Fe I	1.48	-4.708	18	16	27		24		35	38	
6592.91	Fe I	2.73	-1.490	17	97	112	94	112	80	129	134	
6593.87	Fe I	2.43	-2.422	14	72	84	56	84	58	100	102	
6609.11	Fe I	2.56	-2.692	15	37	54	23	49	28	78	81	
6625.02	Fe I	1.01	-5.366	16	13	26		23	11	42	45	
6663.44	Fe I	2.42	-2.479	14	69	85		84				
6677.99	Fe I	2.69	-1.435	17	110	129	94	120	95	140	144	
6750.15	Fe I	2.42	-2.621	14	56	72	44	74	50	97	89	
6752.70	Fe I	4.64	-1.273	19						8	8	
6810.26	Fe I	4.61	-1.003	17		9				15	18	
6945.20	Fe I	2.42	-2.482	14	73	87	57	91	54	113	119	
7112.17	Fe I	2.99	-3.044	19	10	12		12		24	27	
7189.15	Fe I	3.07	-2.825	19	9					28		
7401.69	Fe I	4.19	-1.644	19						16	20	
7511.02	Fe I	4.18	0.082	17	79	92	66	89	71	110	114	
7723.20	Fe I	2.95	-3.617	14	18	34						
5991.38	Fe II	3.15	-3.557	20				14	11	17	20	
6084.11	Fe II	3.20	-3.808	20						10	11	
6149.26	Fe II	3.89	-2.724	20	12	14	12	13	13	19	14	
6247.56	Fe II	3.89	-2.329	20	22	22	20	20	24	34	33	
6416.92	Fe II	3.89	-2.740	20	13	13	11	11			20	
6432.68	Fe II	2.89	-3.708	20	21	24	19	20	19	32	32	
6456.38	Fe II	3.90	-2.075	20	32	37	31	39	36	45	47	
6093.14	Co I	1.74	-2.440	21						17	16	
6117.00	Co I	1.79	-2.490	21						12	12	
6189.00	Co I	1.73	-2.450 -2.450	21						16	17	
6632.43	Co I	2.28	-2.400 -2.000	21						9		
0002.40	001	2.20	2.000	∠ ⊥			-			J		

Table 2—Continued

λ (Å)	Elem.	χ (eV)	$\log gf$	Ref.	1	NGC 628	7	NGC	6293	NGC	6541
					1491	1387	1191	2673	3857	I-44	II-113
6771.04	Co I	1.88	-1.970	21						34	32
6814.94	Co I	1.96	-1.900	21		11		11		29	26
7052.87	Co I	1.96	-1.620	21	23	24		24	13	52	50
7054.05	Co I	2.72	-1.530	21						9	
7417.37	Co I	2.04	-2.070	21		9					
5748.35	Ni I	1.68	-3.260	22				21		33	38
5754.66	Ni I	1.94	-2.330	22		56		49	37	82	
5892.87	Ni I	4.15	-2.350	22		67					
6108.11	Ni I	1.68	-2.450	22	54			64	36		84
6175.36	Ni I	4.09	-0.530	22						18	15
6176.81	Ni I	4.08	-0.530	22						19	23
6177.24	Ni I	4.24	-3.500	22		11				18	14
6256.35	Ni I	1.68	-2.480	22	69	84	53			92	107
6327.59	Ni I	1.68	-3.150	22	28	29		34		51	52
6378.25	Ni I	4.15	-0.890	22							9
6482.80	Ni I	1.94	-2.630	22				31			49
6586.31	Ni I	1.95	-2.810	22	24	25		24	15	49	47
6643.63	Ni I	1.68	-2.300	22	79	99	60	97	58	114	122
6767.77	Ni I	1.83	-2.170	22	73		50	85	59	96	101
6914.56	Ni I	1.95	-2.270	22	53	68		62		89	92
7122.19	Ni I	3.54	0.040	22		68	49			89	91
7197.01	Ni I	1.94	-2.680	22	38					66	86
7261.92	Ni I	1.95	-2.700	22					31		
7414.50	Ni I	1.99	-2.570	22	37	54	25		27	71	73
7422.28	Ni I	3.63	-0.140	22	43	50	31			74	73
7714.31	Ni I	1.94	-2.200	22	72	89	46				
5853.69	Ba II	0.60	-1.010	23	92	114	97	95	75	111	118
6141.73	Ba II	0.70	-0.080	23	147	164	136	141	117	158	169
6496.91	Ba II	0.60	-0.380	23	154	181	142	150	114	162	178
6390.48	La II	0.32	-1.450	24	11	16		10		17	17
6774.27	La II	0.13	-1.820	24	11	13		11		14	18
6645.06	Eu II	1.38	0.204	25	11	16		12	10	16	17
7217.55	Eu II	1.23	-0.301	25	7	8		9		9	

Table 3. References for $\log gf$ values

Ref. No.	Reference	Elem.
1	Lambert (1978)	[O I]
2	Prochaska et al. (2000)	Na I
3	Kraft et al. (1992)	Na I
4	Thévenin (1990)	Mg I
5	Sneden et al. (1997)	Al I
6	Garz (1973)	Si I
7	Smith (1981)	Ca I
8	Blackwell et al. (1982a)	Ti I
9	Blackwell et al. (1983)	Ti I
10	Blackwell et al. (1986b)	Ti I
11	Fuhr et al. (1988a)	Ti II, Cr I
12	Whaling et al. (1985)	VI
13	Blackwell et al. (1979)	Fe I
14	Blackwell et al. (1982b)	Fe I
15	Blackwell et al. (1982c)	Fe I
16	Blackwell et al. (1986a)	Fe I
17	O'Brian et al. (1991)	Fe I
18	Bard et al. (1991)	Fe I
19	Bard & Kock (1994)	Fe I
20	Biémont (1991)	Fe II
21	Cardon (1982)	Co I
22	Fuhr et al. (1988b)	Ni I
23	Sneden et al. (1997)	Ba II
24	Kurucz (1995)	La II
25	Biémont et al. (1982)	Eu II

Table 4. Model atmosphere parameters.

	E(B-V)		Pho	Photometric		pectrosco	opic	$\Delta(\text{Ph.}-\text{Sp.})$	
Id		$(m - M)_0$	T_{eff} (K)	$\frac{\log g}{(0.8M_{\odot})}$	T_{eff} (K)	$\log g$	v_{turb} (km/s)	ΔT_{eff} (K)	$\Delta \log g$
NGC 6287-1491	0.62	14.35	4443	1.0	4375	0.7	1.75	68	0.3
NGC 6287-1387	0.62	14.35	4219	0.8	4250	0.5	1.90	-31	0.3
NGC 6287-1191	0.62	14.35	4493	1.1		0.9	1.80		0.2
NGC 6293-2673	0.40	14.61	4356	0.8	4250	0.5	1.90	106	0.3
NGC 6293-3857	0.40	14.61	4405	1.1	4450	0.7	1.75	-45	0.4
NGC 6541-I-44	0.14	14.19	4271	0.8	4250	0.7	1.85	21	0.1
NGC 6541-II-113	0.14	14.19	4212	0.8	4200	0.5	1.80	11	0.1

Table 5. Radial velocity measurements

Id.		v_r (km s ⁻¹)	$\begin{array}{c} \sigma \\ (\mathrm{km}\;\mathrm{s}^{-1}) \end{array}$	Note
NGC 6287 NGC 6293 NGC 6541	1491 1387 1191 2673 3857 I-44	-290.04 -294.06 -282.31 -158.57 -145.27 -162.52	0.94 0.89 0.67 0.89 0.69 0.43	
	II-113 I-21	-172.49 -34.13	$0.93 \\ 0.79$	Non Member

Table 6. Elemental abundances of NGC 6287.

		1491				1387				1191		
	$\log g_P$	$\log g_S$	σ	n	$\log g_P$	$\log g_S$	σ	n	$\log g_P$	$\log g_S$	σ	n
$[\mathrm{Fe/H}]_{\mathrm{I}}$	-2.17	-2.15	0.09	53	-2.14	-2.10	0.09	53	-2.18	-2.16	0.12	33
$[\mathrm{Fe}/\mathrm{H}]_{\mathrm{II}}$	-1.99	-2.11	0.05	5	-1.95	-2.09	0.06	5	-2.08	-2.16	0.07	5
$[\mathrm{Fe}/\mathrm{H}]_{avg}$		-2.13	0.10			-2.10	0.11			-2.16	0.04	
[O/Fe]	0.34	0.37	0.01	2	0.24	0.28	0.01	2	0.34	0.39		1
[Na/Fe]	0.28	0.26		1	0.71	0.72	0.03	3				
[Mg/Fe]	0.26	0.24		1	0.44	0.44	0.01	2				
[Al/Fe]					0.93	0.88	0.00	2				
[Si/Fe]	0.57	0.51	0.05	2	0.52	0.46	0.05	6				
[Ca/Fe]	0.22	0.21	0.10	17	0.16	0.17	0.08	16	0.24	0.17	0.06	7
$[\mathrm{Ti}/\mathrm{Fe}]_{\mathrm{I}}$	0.19	0.18	0.08	8	0.02	0.06	0.06	9				
$[\mathrm{Ti}/\mathrm{Fe}]_{\mathrm{II}}$	0.16	0.18	0.05	2	0.11	0.10	0.01	2				
[V/Fe]	-0.02	-0.03	0.01	3	-0.09	-0.05	0.04	2				
[Cr/Fe]	-0.14	-0.16	0.02	2	-0.11	-0.10	0.04	2				
[Co/Fe]	0.27	0.25		1	0.07	0.06	0.07	3				
[Ni/Fe]	0.09	0.05	0.09	11	0.04	0.01	0.12	12	-0.02	-0.03	0.10	7
$[\mathrm{Ba/Fe}]_{\mathrm{II}}$	0.34	0.38	0.18	3	0.43	0.49	0.16	3	0.39	0.40	0.09	3
$[La/Fe]_{II}$	0.30	0.32	0.06	2	0.26	0.30	0.02	2				
$[\mathrm{Eu}/\mathrm{Fe}]_{\mathrm{II}}$	0.45	0.47	0.02	2	0.44	0.47	0.04	2		• • •	• • •	

Table 7. Elemental abundances of NGC 6293.

		2673				3857		
	$\log g_P$	$\log g_S$	σ	n	$\log g_P$	$\log g_S$	σ	n
$[\mathrm{Fe/H}]_{\mathrm{I}}$	-2.16	-2.16	0.10	54	-2.20	-2.18	0.09	45
$[\mathrm{Fe}/\mathrm{H}]_{\mathrm{II}}$	-1.99	-2.12	0.08	6	-1.99	-2.15	0.04	5
$[{\rm Fe}/{\rm H}]_{avg}$	• • •	-2.10	0.14	• • •		-2.17	0.10	• • •
[O/Fe]					-0.14	-0.09		1
[Na/Fe]	0.40	0.41	0.06	2	0.38	0.40		1
[Mg/Fe]	-0.26	-0.25		1	0.17	0.14		1
[Al/Fe]	1.01	1.01	0.04	2	0.97	0.97		1
[Si/Fe]	0.68	0.61	0.06	6	0.54	0.51	0.10	2
[Ca/Fe]	0.22	0.23	0.10	14	0.23	0.24	0.07	14
$[\mathrm{Ti}/\mathrm{Fe}]_{\mathrm{I}}$	0.08	0.09	0.11	4	0.12	0.14	0.08	4
$[\mathrm{Ti}/\mathrm{Fe}]_{\mathrm{II}}$	0.09	0.13		1	0.14	0.16	0.21	2
[V/Fe]	-0.15	-0.15	0.06	7	0.28	0.30	0.03	2
[Cr/Fe]	-0.17	-0.17	0.03	2	-0.10	-0.09	0.01	2
[Co/Fe]	0.06	0.03	0.05	2	0.15	0.15		1
[Ni/Fe]	-0.04	-0.07	0.09	9	-0.03	-0.03	0.09	7
$[\mathrm{Ba/Fe}]_{\mathrm{II}}$	0.07	0.16	0.09	3	-0.07	-0.07	0.01	3
$[\mathrm{La/Fe}]_{\mathrm{II}}$	0.15	0.18	0.08	2				
$[\mathrm{Eu}/\mathrm{Fe}]_\mathrm{II}$	0.43	0.46	0.08	2	0.41	0.45		1

Table 8. Elemental abundances of NGC 6541.

		I-44				II-113		
	$\log g_P$	$\log g_S$	σ	n	$\log g_P$	$\log g_S$	σ	n
$[\mathrm{Fe}/\mathrm{H}]_\mathrm{I}$	-1.85	-1.85	0.08	47	-1.86	-1.86	0.08	47
$[\mathrm{Fe}/\mathrm{H}]_{\mathrm{II}}$	-1.79	-1.83	0.07	6	-1.72	-1.85	0.08	7
$[{\rm Fe}/{\rm H}]_{avg}$	• • •	-1.84	0.11		• • •	-1.86	0.11	
[O/Fe]	-0.58	-0.55		1	-0.09	-0.07	0.05	2
[Na/Fe]	0.40	0.40	0.00	2	0.26	0.29	0.04	2
[Mg/Fe]					0.34	0.36	0.02	2
[Al/Fe]	1.33	1.30		1	1.02	1.05	0.01	2
[Si/Fe]	0.51	0.51	0.06	4	0.52	0.56	0.08	4
[Ca/Fe]	0.31	0.32	0.08	10	0.36	0.39	0.09	11
$[\mathrm{Ti}/\mathrm{Fe}]_{\mathrm{I}}$	0.22	0.22	0.07	15	0.17	0.20	0.06	12
$[\mathrm{Ti}/\mathrm{Fe}]_{\mathrm{II}}$	0.27	0.28	0.01	2	0.17	0.19	0.02	2
[V/Fe]	-0.09	-0.09	0.07	12	-0.10	-0.07	0.07	11
[Cr/Fe]	0.25	0.25	0.01	2	-0.05	-0.02	0.03	3
[Co/Fe]	0.20	0.19	0.06	6	0.11	0.11	0.05	4
[Ni/Fe]	0.02	0.01	0.08	15	0.01	-0.01	0.15	17
$[\mathrm{Ba/Fe}]_{\mathrm{II}}$	0.17	0.19	0.06	3	0.29	0.34	0.09	3
$[{\rm La/Fe}]_{\rm II}$	0.14	0.15	0.01	2	0.12	0.14	0.09	2
$[\mathrm{Eu}/\mathrm{Fe}]_{\mathrm{II}}$	0.32	0.31	0.04	2	0.29	0.30		1

Table 9. Mean elemental abundances of program clusters.

	NGC	6287	NGC 6	5293	NGC	6541
	$\log g_P$	σ	$\log g_P$	σ	$\log g_P$	σ
$[\mathrm{Fe/H}]_{\mathrm{II}}$	-2.01	0.06	-1.99	0.00	-1.76	0.04
[O/Fe]	0.31	0.06	-0.14*		-0.33	0.25
[Na/Fe]	0.50	0.22	0.39	0.01	0.33	0.07
[Mg/Fe]	0.35	0.09	-0.04	0.22	0.34*	
[Al/Fe]	0.93*		0.99	0.02	1.18	0.16
[Si/Fe]	0.55	0.03	0.61	0.07	0.52	0.01
[Ca/Fe]	0.21	0.04	0.23	0.01	0.34	0.04
$[\mathrm{Ti}/\mathrm{Fe}]_{\mathrm{I}}$	0.11	0.09	0.10	0.02	0.20	0.03
$[\mathrm{Ti}/\mathrm{Fe}]_{\mathrm{II}}$	0.14	0.03	0.12	0.03	0.22	0.05
[V/Fe]	-0.05	0.04	0.07	0.22	-0.09	0.01
[Cr/Fe]	-0.12	0.02	-0.13	0.04	0.10	0.15
[Co/Fe]	0.17	0.10	0.11	0.05	0.16	0.05
[Ni/Fe]	0.04	0.06	-0.03	0.01	0.02	0.01
$[Ba/Fe]_{II}$	0.39	0.05	0.00	0.07	0.23	0.06
$[La/Fe]_{II}$	0.28	0.02	0.15^{*}		0.13	0.01
[Eu/Fe] _{II}	0.45	0.01	0.42	0.01	0.31	0.02

 $^{{\}rm *Single\ star\ measurement}.$

Table 10. Abundance dependencies on model atmosphere.

	δT_{eff}		δlo	$\delta \log g$		δv_{turb}		$\delta T_{eff}/\delta \log g/\delta v_{turb}$	
	-100	+100	-0.3	+0.3	-0.3	+0.3	-100	+100	
	(K)	(K)			(km/s)	(km/s)	-0.1	+0.1	
							-0.1	+0.1	
$[\mathrm{Fe}/\mathrm{H}]_\mathrm{I}$	-0.11	0.13	0.00	0.01	0.07	-0.06	-0.09	0.10	
$[\mathrm{Fe}/\mathrm{H}]_{\mathrm{II}}$	0.10	-0.08	-0.13	0.15	0.03	-0.02	0.05	-0.05	
[O/Fe]	-0.14	0.09	0.02	-0.03	-0.04	0.01	-0.13	0.10	
[Na/Fe]	0.01	-0.03	0.03	-0.04	-0.07	0.05	0.00	-0.02	
[Mg/Fe]	0.03	-0.06	0.01	-0.03	-0.05	0.03	0.03	-0.05	
[Al/Fe]	0.01	-0.03	0.03	-0.03	-0.06	0.05	0.01	-0.02	
[Si/Fe]	0.13	-0.13	-0.04	0.04	-0.06	0.04	0.11	-0.11	
[Ca/Fe]	-0.03	0.01	0.02	-0.04	0.05	-0.05	-0.01	0.01	
$[\mathrm{Ti}/\mathrm{Fe}]_{\mathrm{I}}$	-0.09	0.08	0.03	-0.03	-0.04	0.04	-0.09	0.08	
$[\mathrm{Ti}/\mathrm{Fe}]_{\mathrm{II}}$	-0.06	0.04	0.01	-0.02	-0.02	0.02	-0.05	0.05	
[V/Fe]	-0.11	0.10	0.03	-0.02	-0.05	0.05	-0.11	0.10	
[Cr/Fe]	-0.03	0.01	0.02	-0.03	-0.04	0.04	-0.03	0.02	
[Co/Fe]	-0.02	0.02	-0.01	0.02	-0.05	0.05	-0.03	0.04	
[Ni/Fe]	0.02	-0.01	-0.02	0.03	0.03	-0.01	0.01	-0.01	
[Ba/Fe]	-0.13	0.12	0.04	-0.06	0.25	-0.23	-0.07	0.03	
[La/Fe]	-0.11	0.11	0.02	-0.02	-0.01	0.02	-0.10	0.10	
[Eu/Fe]	-0.10	0.07	0.01	-0.02	-0.02	0.01	-0.08	0.07	
[Si I/Ti I]	0.23	-0.21	-0.06	0.06	-0.02	0.01	0.20	-0.18	
[Si I/Ti II]	-0.01	0.03	0.09	-0.08	0.00	0.00	0.01	0.00	

Table 11. α -element abundances

Id.	[Si/Fe]	[Ca/Fe]	[Ti/Fe]	$[\alpha/\mathrm{Fe}]$	n^1
NGC 6287	0.55 ± 0.03	0.21 ± 0.04	0.12 ± 0.07	0.30 ± 0.02	
NGC 6293	0.61 ± 0.07	0.23 ± 0.01	0.11 ± 0.03	0.32 ± 0.02	
NGC 6541	0.52 ± 0.01	0.34 ± 0.04	0.21 ± 0.05	0.36 ± 0.02	
old halo	0.38 ± 0.05	0.30 ± 0.03	0.33 ± 0.03	0.34 ± 0.02	15
younger halo	0.29 ± 0.09	0.14 ± 0.06	0.17 ± 0.07	0.20 ± 0.05	7
younger halo ²	0.38 ± 0.09	0.21 ± 0.04	0.25 ± 0.06	0.28 ± 0.02	5
disk	0.39 ± 0.08	0.16 ± 0.07	0.31 ± 0.08	0.29 ± 0.10	4

 $^{^1\}mathrm{Number}$ of clusters.

²Without Palomar 12 and Rupercht 106.

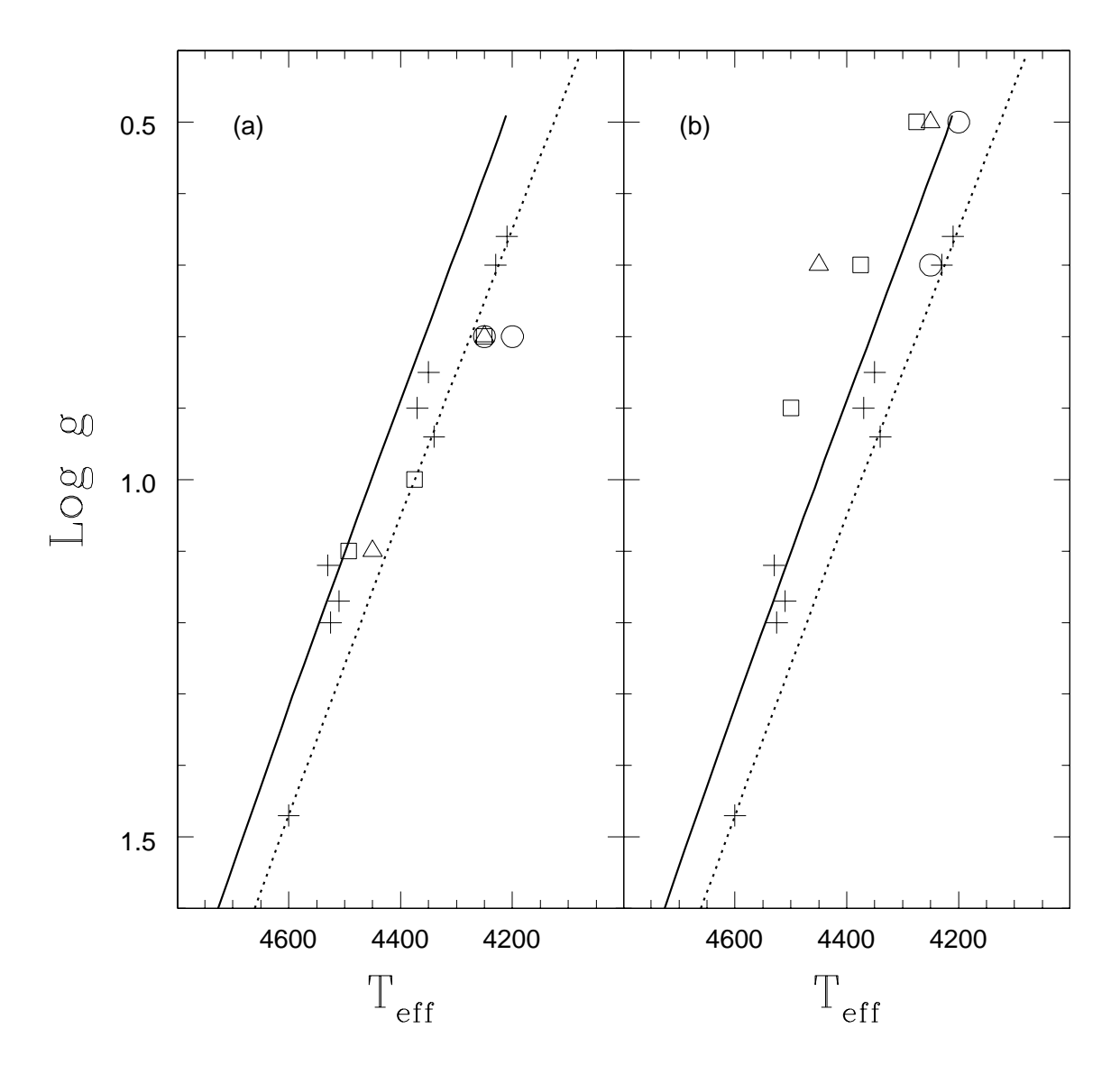


Fig. 1.— Comparisons of the model atmosphere parameters to the model isochrones using photometric surface gravities (a) and spectroscopic surface gravities (b). The open squares represent the NGC 6287 RGB stars, the open triangles the NGC 6293 RGB stars, and the open circles the NGC 6541 RGB stars. We also show the M92 RGB stars (Sneden et al. 1991) with crosses. The solid lines is for the model isochrone with [Fe/H] = -2.14 and the dotted lines for that with [Fe/H] = -1.84 (Bergbusch & VandenBerg 2001).

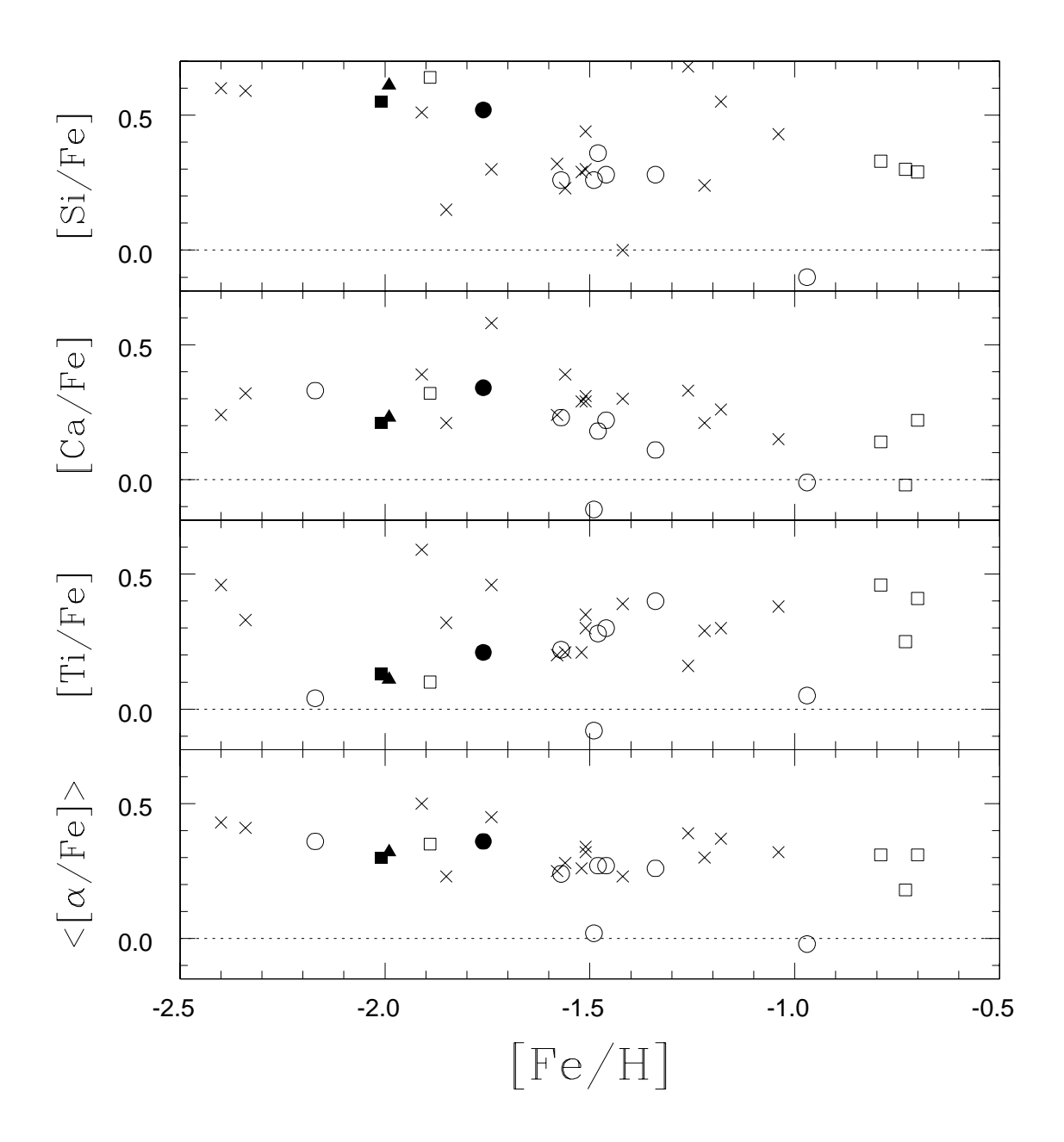


Fig. 2.— α -element abundances for globular clusters. Crosses represent "old halo" clusters, open circles "younger halo" clusters, and open squares "thick disk" clusters. NGC 6287 is represented by filled squares, NGC 6293 by filled triangles, and NGC 6541 by filled circles. Our program clusters appear to be silicon enhanced and titanium deficient.

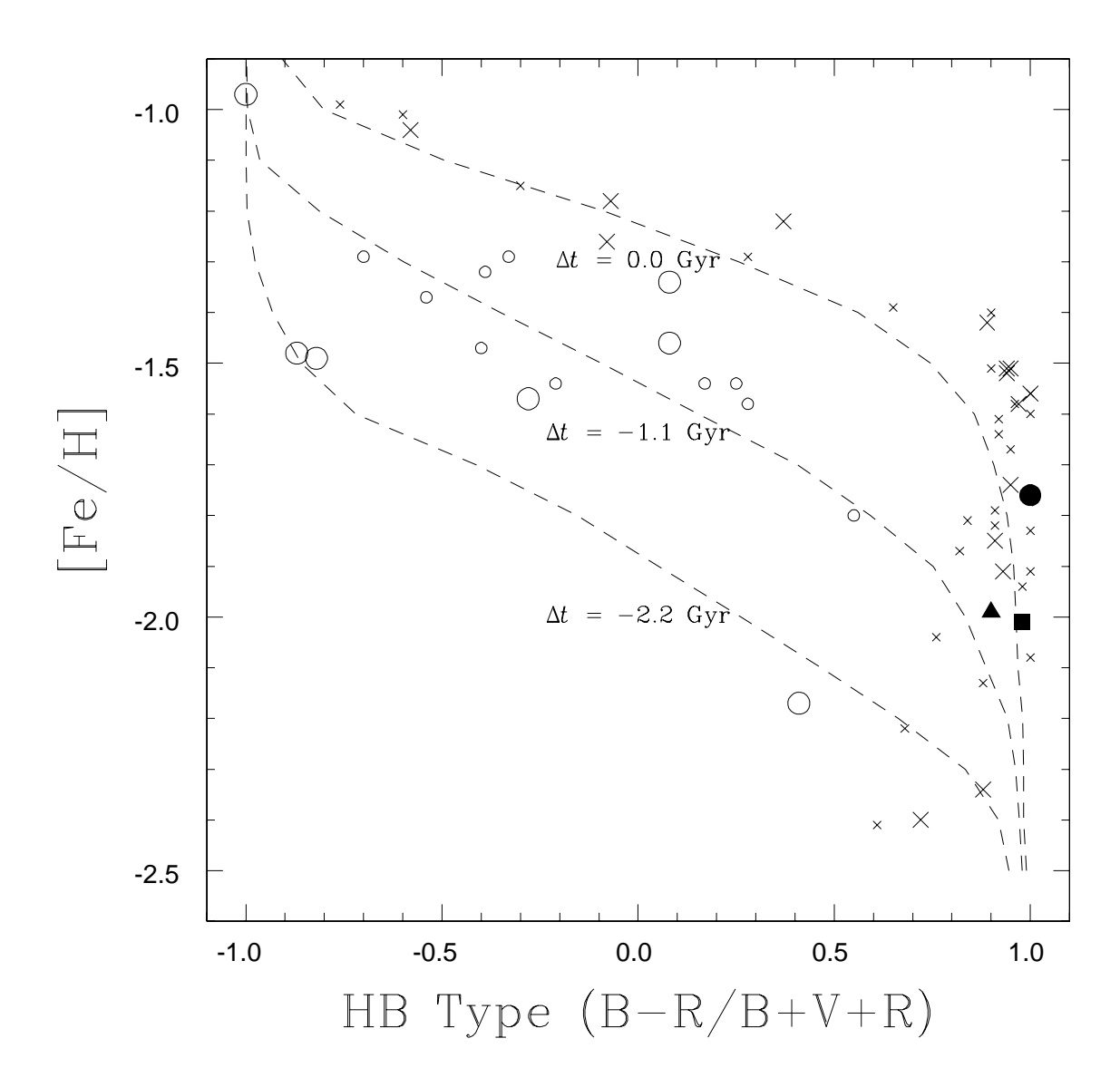


Fig. 3.— HB type versus [Fe/H] (HB isochrones) of "halo" globular clusters (Da Costa & Armandroff 1995) and our program clusters. Crosses are "old halo" clusters and open circles are "younger halo" clusters, where large crosses and open circles denote clusters studied employing high-resolution spectroscopy (see also Figure 2). NGC 6287 is represented by filled squares, NGC 6293 by filled triangles, and NGC 6541 by filled circles. HB isochrones for $\Delta t = 0.0, -1.1$, and -2.2 Gyr (with respect to the mean age of "old halo" globular clusters) are also shown with dashed lines (Rey et al. 2001).

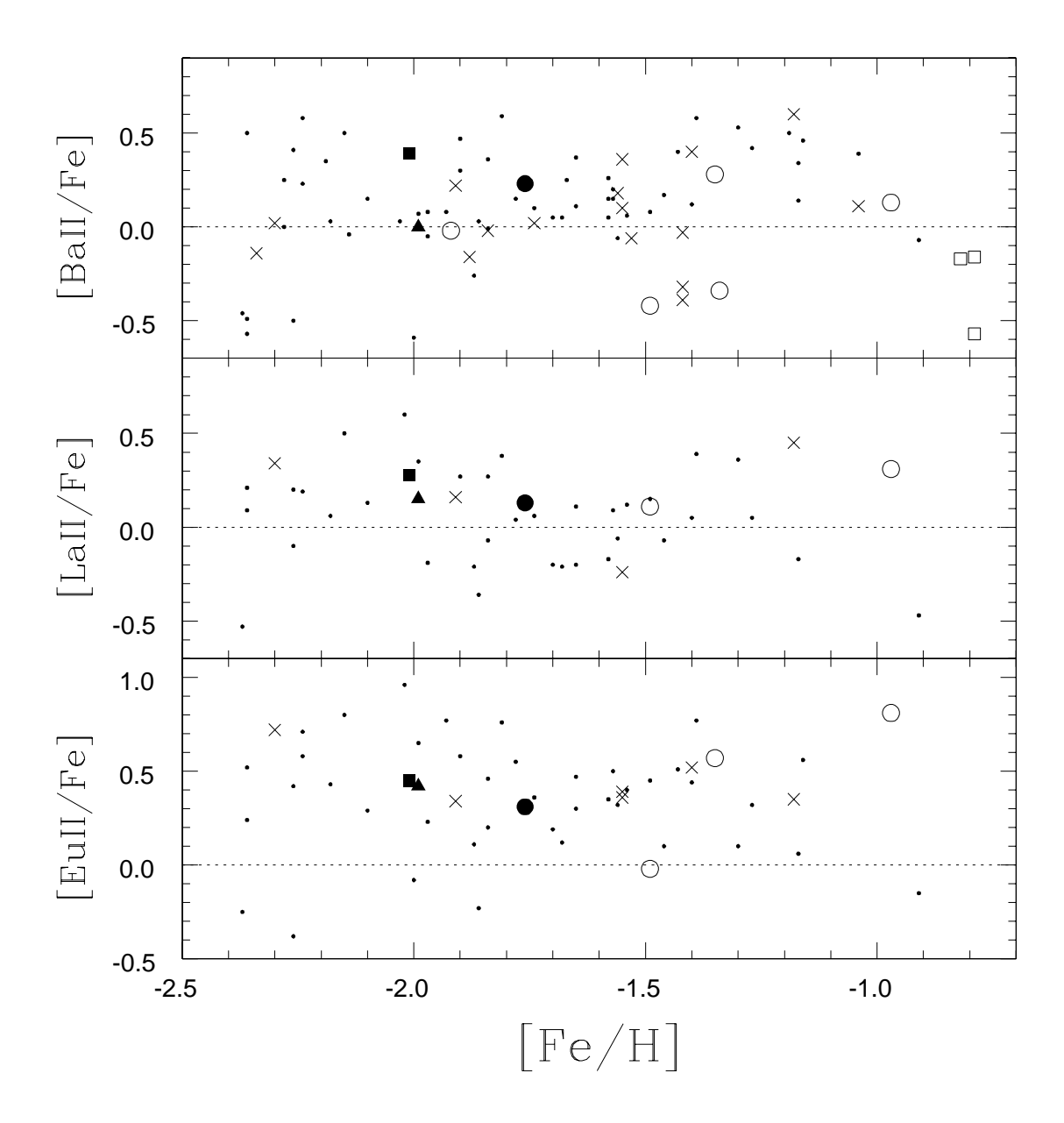


Fig. 4.— Abundances of the neutron capture elements. Crosses are "old halo" clusters, open circles "younger halo" clusters, open squares "thick disk" clusters, and dots the field stars (Burris et al. 2000). NGC 6287 is represented by filled squares, NGC 6293 by filled triangles, and NGC 6541 by filled circles.

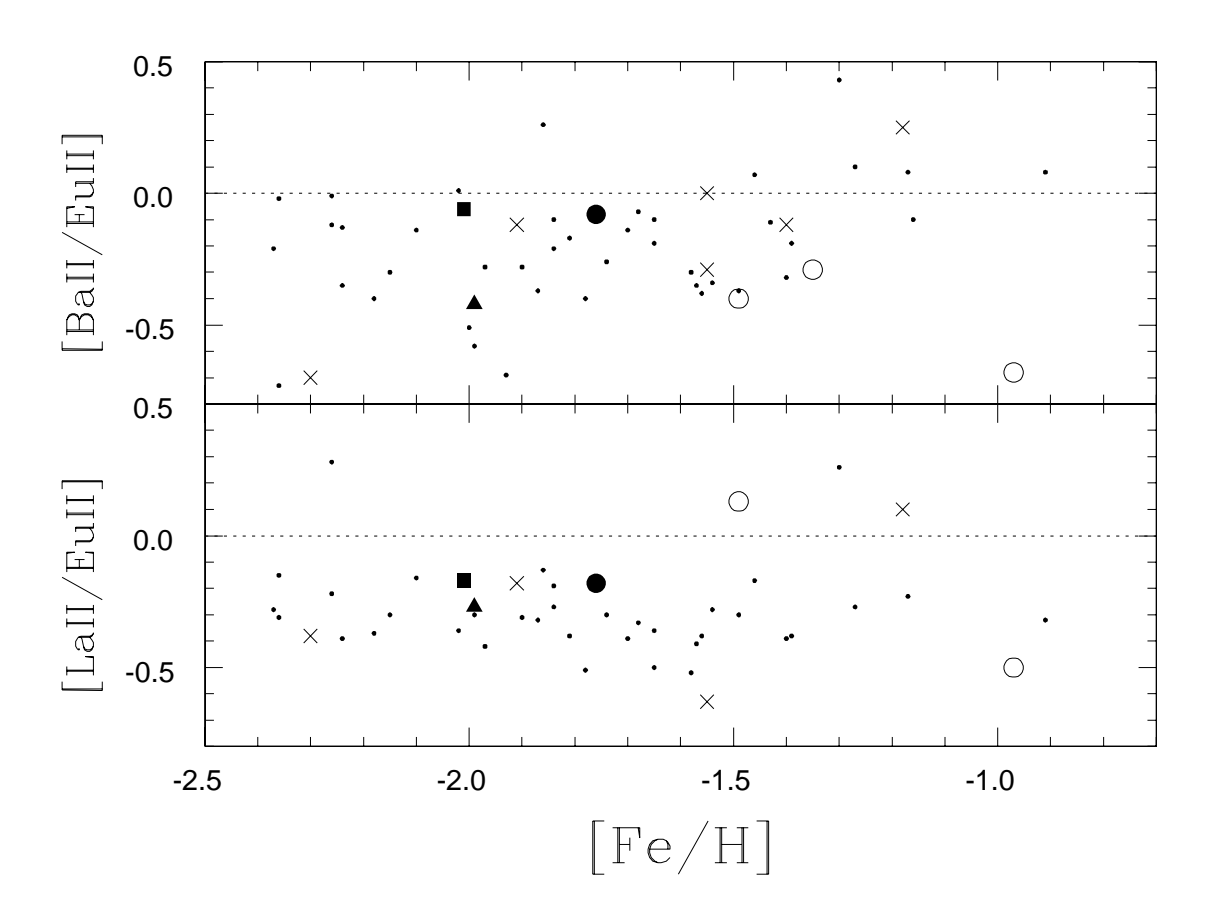


Fig. 5.— Elemental ratios of the neutron capture elements. Crosses are "old halo" clusters, open circles "younger halo" clusters, open squares "thick disk" clusters, and dots the field stars. NGC 6287 is represented by filled squares, NGC 6293 by filled triangles, and NGC 6541 by filled circles.

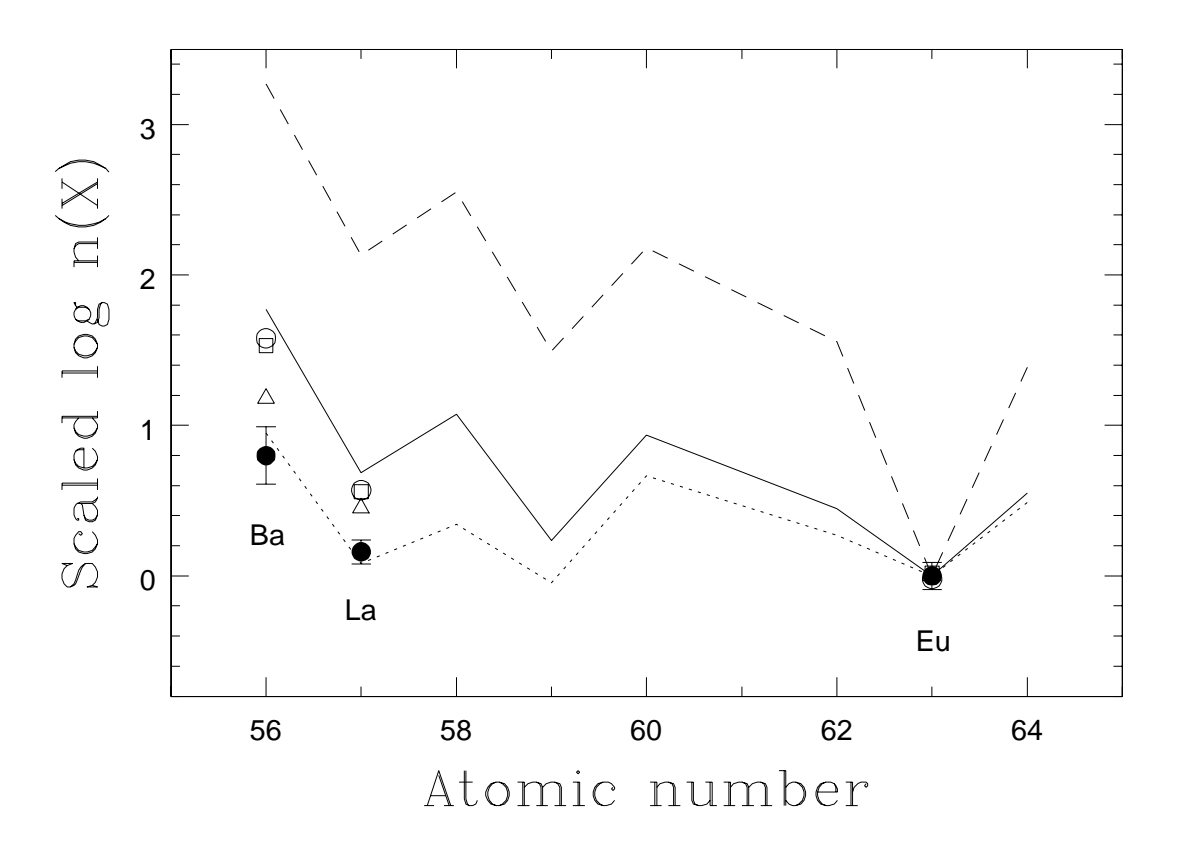


Fig. 6.— Comparisons of the neutron capture elemental abundances to those of the Sun. Ba and La abundances are scaled to match Eu abundances. Open squares are for NGC 6287, open triangles NGC 6293, and open circles NGC 6541. M15 neutron capture elements are also plotted by filled circles (Sneden et al. 2000a). The solid line represents the solar abundances, the dotted line the solar r-process abundances, and the dashed line the solar s-process abundances.

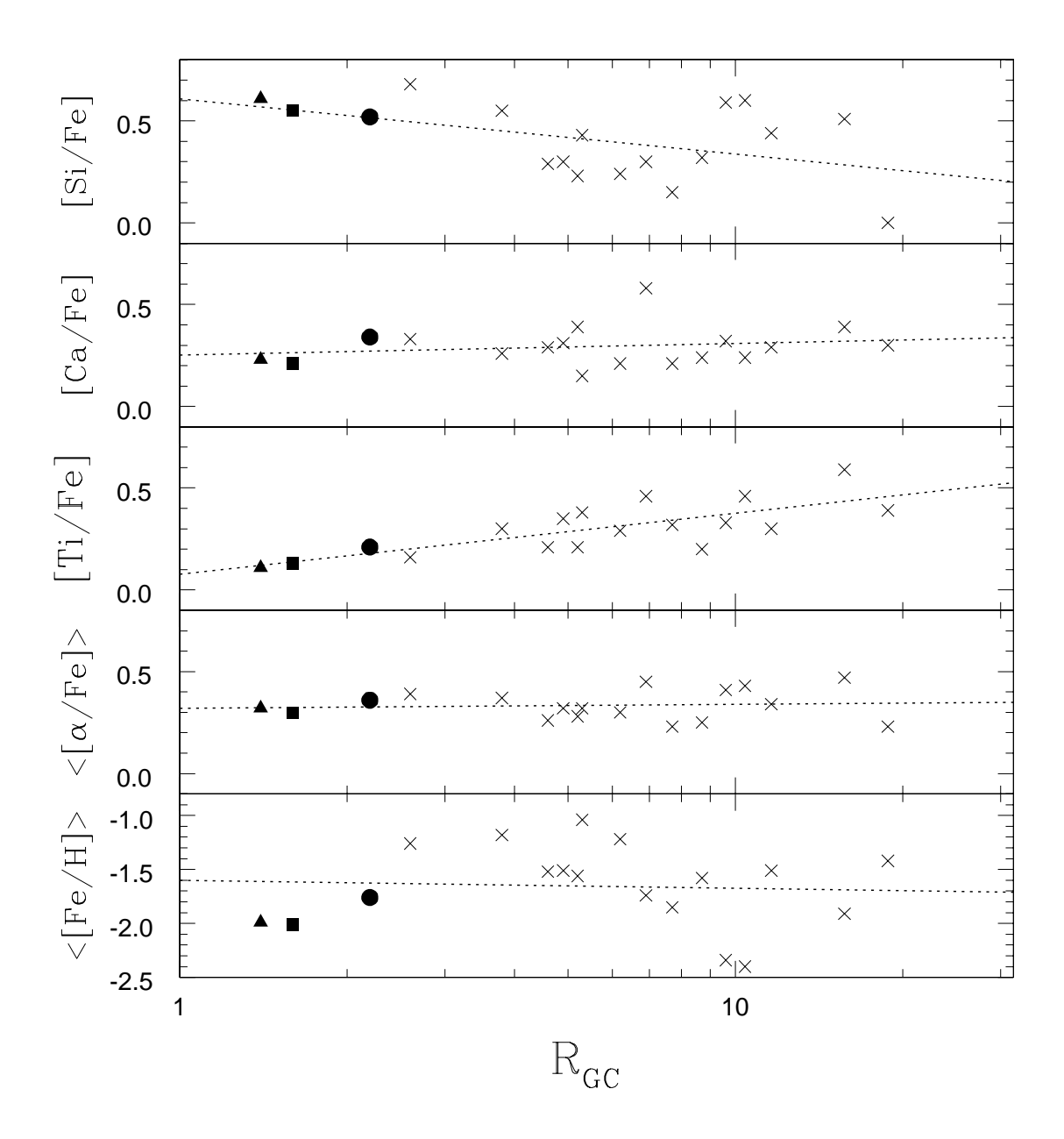


Fig. 7.— The α -element abundances and metallicities of "old halo" clusters as a function of R_{GC} . NGC 6287 is represented by filled squares, NGC 6293 by filled triangles, and NGC 6541 by filled circles. The dotted lines represent the linear fit to the data. Note that metallicities do not reflect the underlying stellar population, but only the objects studied in our study.

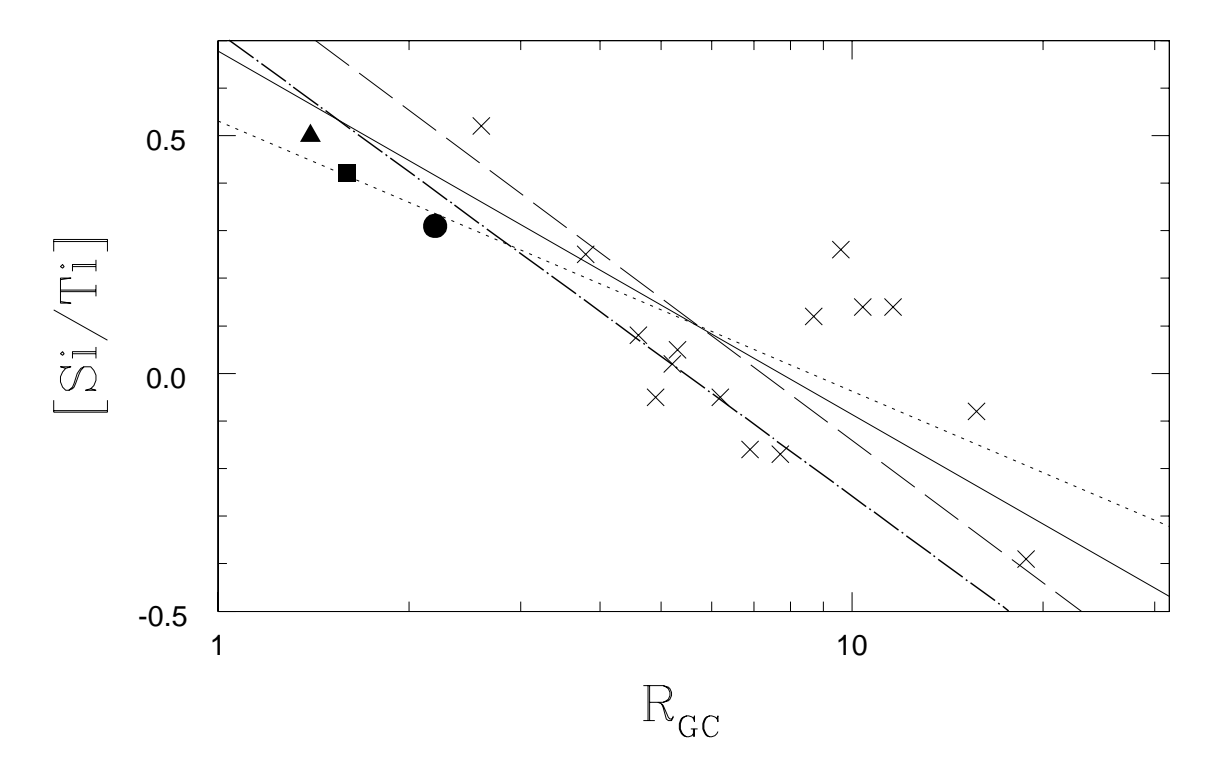


Fig. 8.— [Si/Ti] as a function of R_{GC} . Crosses represent "old halo" clusters. NGC 6287 is represented by filled squares, NGC 6293 by filled triangles, and NGC 6541 by filled circles. The dotted line is for the linear fit, the dashed line for the inverse linear fit, and the solid line for the bisector linear fit to the data. The dashed-dotted line represents the bisector linear fit to the clusters with $R_{GC} \leq 8$ kpc (12 clusters).

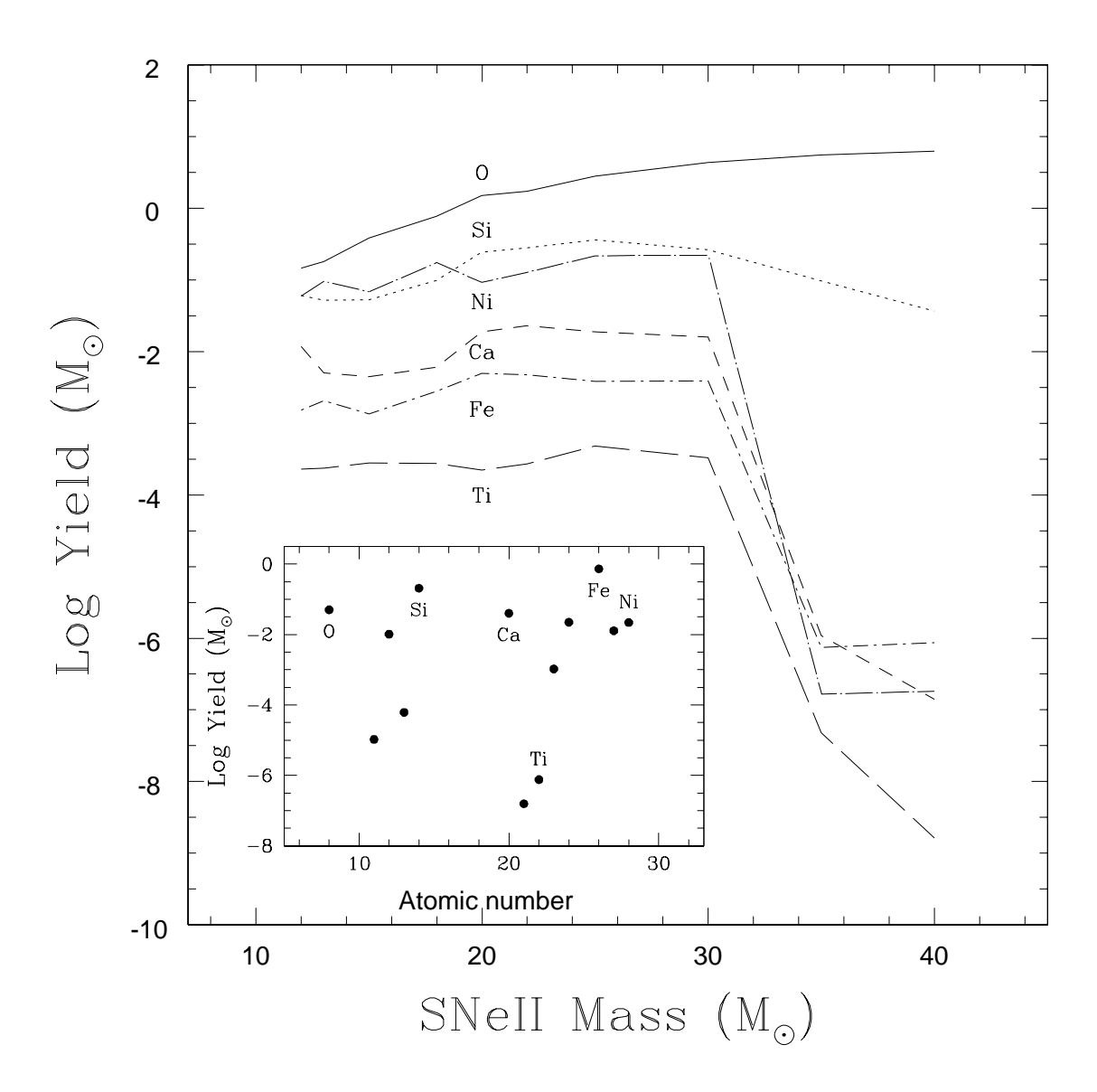


Fig. 9.— SNe II yields as a function of a progenitor mass (Woosley & Weaver 1995). SNe Ia yields as a function of atomic mass are also plotted in the inset. For SNe Ia, we adopt data from Höeflich, Wheeler, & Thielemann (1998).